Molecular recognition mechanism of novel KIR2DS1 specific monoclonal antibodies

（新規ＫＩＲ２ＤＳ１特異的モノクローナル抗体の分子認識機構の解析）

JIANG XINXIN

蒋　欣欣

LABORATORY OF BIOMOLECULAR SCIENCE

BIOMEDICAL AND PHARMACEUTICAL SCIENCE COURSE

GRADUATE SCHOOL OF LIFE SCIENCE

HOKKAIDO UNIVERSITY

September 2020

Contents

Abstract iii
Abbreviations iv
Abbreviations of amino acids vi
Unit vii
Introduction 1
1. Natural killer (NK) cells 1
2. KIRs 2
3. *KIR* genes and haplotypes 3
4. Ligands of KIRs 5
5. Crystal structures of KIRs 7
6. KIR and human diseases 9
7. Anti-KIR monoclonal antibodies (mAbs) 10
8. Novel rat anti-KIR2DS1 specific mAbs 11
Objectives 14
Materials and methods 15
1. Preparation of recombinant KIR2DS1 protein 15
2. Purification of monoclonal antibodies and their Fab fragments 16
3. Surface plasmon resonance (SPR) analyses 17
4. Crystallization and structure determination of KIR2DS1 20
5. Crystallization and structure determination of 1C7 Fab 21
Results 22
1. Structural analysis of KIR2DS1 22
1-1. Preparation of KIR2DS1 recombinant protein 22
1-2. The crystallization and structural determination of KIR2DS1 24
2. The binding properties of three clones with KIR2DS1 protein 27
2-1 The preparation of anti-KIR2DS1 specific mAbs and their Fab fragments 27
2-2. The kinetic analysis of mAbs-KIR2DS1 using SPR 29
2-3. The binding of Fabs to KIR2DS1 protein 31
2-4. Thermodynamic analysis of three Fabs and KIR2DS1 interaction 34
3. The structural analysis of 1C7 Fab 37
Discussion 40

References **45**
Acknowledgements **51**

Abstract

Natural killer (NK) cells play critical roles in host defense against tumors, microbial infections, hematopoietic and solid organ transplantations and autoimmune diseases. The activation of NK cell functions is regulated by multiple types of activating and inhibitory receptors designated as paired receptors which recognize the cell surface ligands on potential target cells. Killer cell immunoglobulin-like receptor (KIR) family consists of polymorphic but highly homologous paired receptors and regulates human NK cell functions. Especially, two paired receptors against human leukocyte antigen (HLA)-C allotypes with K80, activating KIR2DS1 and inhibitory KIR2DL1, have only six different amino acid residues, and hard to be discriminated by monoclonal antibodies (mAbs). In our laboratory, three novel rat anti-KIR2DS1 specific mAbs (1C7, 5B12, and 3E11) were successfully generated. These mAbs showed high specificity to KIR2DS1. All three mAbs recognized the N163 residue of KIR2DS1 by the mutation assay using surface plasmon resonance (SPR) analysis. Interestingly, only 1C7 mAb additionally recognized T154 residue.

These specific mAbs against KIR2DS1 are expected to be used for the basic research to clarify the expression properties of KIR2DS1 in the NK cell-related immune disorders, and to be developed as a candidate for therapeutic antibody drug as well. In this study, I analyzed the molecular recognition mechanism of three novel anti-KIR2DS1 mAbs for future clinical applications in the effective regulation of NK cell functions.

Abbreviations

2xYT	2x yeast extract tryptone medium
2-ME	2-mercaptoethanol
AEC	Anion exchange chromatography
AML	Acute myeloid leukemia
Cen	Centromeric
CMV	Cytomegaloviruses
D	Domain
DNA	Deoxyribonucleic acid
DTT	Dithiothreitol
DAP12	DNAX activating protein of 12 kDa
E.coli	Escherichia coli
EDTA	Ethylenediaminetetraacetic acid
ELISA	Enzyme-linked immunosorbent assay
Fab	Antibody binding fragment
FBS	Fetal bovine serum
FcRγ	Fc receptor common γ chain
HCl	Hydrochloride
HCV	Hepatitis C virus
HEPES	4-(2-hydroxyethyl)-1-piperazineethanesulfonic acid
HIV	Human immunodeficiency virus
HLA	Human leukocyte antigen
IPTG	Isopropyl β-D-1-thiogalactopyranoside
ITAM	Immunoreceptor tyrosine-based activating motif
ITIM	Immunoreceptor tyrosine-based inhibitory motif
Ig	Immunoglobulin
KIR	Killer cell immunoglobulin-like receptor
LILR	Leukocyte immunoglobulin-like receptor
LB	Lysogeny broth
LRC	Leukocyte receptor complex
mAb	Monoclonal antibody
MDS	Myelodysplastic syndromes
MW	Molecular weight

MM	Multiple myeloma
NK	Natural killer
NCR	Natural cytotoxicity receptors
NaCl	Sodium chloride
OD	Optical density
PAGE	Polyacrylamide gel electrophoresis
PCR	Polymerase chain reaction
PDB	The protein data bank
PEG	Polyethylene glycol
RA	Rheumatoid arthritis
RNA	Ribonucleic acid
S	Short
SDS	Sodium dodecyl sulfate
SEC	Size exclusion chromatography
SHP	Src-homology 2 domain-containing protein tyrosine phosphatase
SHIP	Src-homology 2 domain-containing inositol-phosphatase
SPR	Surface plasmon resonance
TCR	T cell receptor
Tel	Telomeric
TM	Transmembrane
Tris	Tris (hydroxymethyl) aminomethane
Triton X-100	Polyoxyethylene (10) octylphenyl ether
VH	Variable heavy chain
VL	Variable light chain
w/v	Weight per volume
β2m	Beta 2-microglobulin

Abbreviations of amino acids

Alanine	A
Arginine	R
Asparagine	N
Aspartic acid	D
Cysteine	C
Glutamic acid	E
Glutamine	Q
Glycine	G
Histidine	H
Isoleucine	I
Leucine	L
Lysine	K
Methionine	M
Phenylalanine	F
Proline	P
Serine	S
Threonine	T
Tryptophan	W
Tyrosine	Y
Valine	V

Unit

°C	Degree Celsius (0°C = 273.15 K)
min	Minute (1 min = 60 s)
L	Liter (1 L = 10-3 m3)
M	Molar (M = mol/L)
AU	Absorbance unit
KD	Affinity constant
rpm	Revolutions per minute
RU	Response unit
pH	Power of hydrogen

Introduction

1. Natural killer (NK) cells

NK cells are large lymphocytes with a distinctive granular cytoplasm. NK cells play critical roles in the innate immune system and are suggested to be associated with various types of diseases such as tumors, microbial infections, solid organ transplantations and autoimmune diseases [1]. Different from B cells and T cells, which express antigen-specific receptors and play important roles in the adaptive immune system, NK cells do not require antigen-specific recognition for their activation. NK cells are mainly regulated by the signaling pathways through the NK cell receptors for human leukocyte antigen (HLA) class I molecules on the target cells (Table 1) [2]. According to the "missing self-hypothesis" [3], the normal healthy cells expressing HLA class I molecules with self-peptides could be survived from NK cell killing, whereas non-healthy cells, such as tumor or virus-infected cells, have lost HLA class I surface molecules and can be cytolytically attacked by NK cells with a large array of perforins and endogenous granzymes.

NK cell activation in human is controlled by a balance regulated by the paired cell surface receptors. Paired receptors consist of activating and inhibitory receptors sharing significantly conserved amino acid sequences within the extracellular domains to potentially recognize the same ligand, and regulate the cell functions [4]. The main paired receptors on the NK cell surface are killer immunoglobulin-like receptors (KIRs) and natural cytotoxicity receptors (NCRs). The NCR family is comprised of three type I transmembrane (TM) receptors, NKp46, NKp44, and NKp30, which are encoded by the genes, *NCR1*, *NCR2*, and *NCR3*, respectively [5]. The inhibitory and activating NK cell receptors regulate the NK cell functions by the balance in the signaling depending on the expression levels of both the ligands on the target cells and receptors themselves. Most of the immature NK cells express the important inhibitory receptor, the CD94:NKG2A heterodimer, specific for the non-classical HLA class I molecule, HLA-E, which presents a peptide derived from a leader sequence of other HLA class I molecules. On the other hand, KIRs are expressed at the late stages of NK cell differentiation. CD94:NKG2A co-expressed with KIRs at a further differentiation stage might cooperatively regulate with KIR on NK cell activation. A member of leukocyte Ig-like receptors (LILR) family, LILRB1, and leukocyte-associated Ig-like receptors (LAIRs) are also expressed in NK cells and transmit the inhibitory signals by recognizing self-ligands [6].

Table 1. Examples of NK cell receptors.

	Gene locus	Domain types	Ligands
Activating			
CD16	1q23	Ig-like	IgG [7]
NKp44	6p21	Ig-like	Influenza haemagglutinin [8]
NKp30	6p21	Ig-like	Unknown
NKp46	19q13	Ig-like	Influenza haemagglutinin [8]
KIR2DS1-2, 4	19q13	Ig-like	HLA class I allotypes [9]
NKG2D	12p12	C-type lectin like	MICA, MICB, ULBPs [10, 11]
CD94/NKG2C	12p12	C-type lectin like	HLA-E [12, 13]
Inhibitory			
KIR2DL1-3, 3DL1-2	19q13	Ig-like	HLA class I allotypes [9]
CD94/NKG2A	12p12	C-type lectin like	HLA-E [13, 14]
LILRB1	19q13	Ig-like	HLA class I [15]
LAIR1, LAIR2	19q13	Ig-like	Unknown

2. KIRs

KIR (CD158) family is one of the paired receptors expressed in NK cells and subsets of T cells. The KIR nomenclature was determined by their domain structure and the function (Figure 1). For example, KIR2DS1 possesses two extracellular domains (2D) and short cytoplasmic tail (S), and KIR3DL1 possesses three extracellular domains (3D) and long cytoplasmic tail (L). The length of the cytoplasmic tail determines the function of KIRs. KIR family has two pseudogenes namely KIR2DP1 and KIR3DP1 (Figure 2) [16]. Each Ig-like extracellular domain of KIRs was defined as D0, D1, and D2 based on their sequence similarities (Figure 1). All KIR3D molecules have the D0-D1-D2 configuration (from N to C terminus). KIR2D molecules have either D1- D2 (type I) or D0-D2 (type II) configuration [16].

KIRs with long cytoplasmic tails KIR-L (KIR2DLs and KIR3DLs) transmit the inhibitory signals through one or more immunoreceptor tyrosine-based inhibition motifs (ITIMs; I/S/T/LxYxxL/V) [16]. Once inhibitory KIRs interact with HLA class I molecules on the target cells, the tyrosine residue of ITIMs becomes phosphorylated by Src kinase family molecules and then recruit other enzymes such as the phosphotyrosine phosphatases SHP-1 and SHP-2, or the inositol-phosphatase called SHIP. These signals result in the inhibition of cell activation

and proliferation. In contrast, the KIRs with short cytoplasmic tail, KIR-S (KIR2DSs and KIR3DSs) possess a charged residue (lysine) in their TM region which associates with the signaling adaptor protein, DNAX activating protein of 12 kDa (DAP12) containing immunoreceptor tyrosine-based activating motifs (ITAMs). Interestingly, KIR2DL4 has unique features, an ITIM in the long cytoplasmic tail and a charged residue (arginine) in the TM region allowing its association with the γ chain of FcεR (Figure 1). With such an unusual hybrid structure, KIR2DL4 was reported to have a weak inhibitory potential and to induce strong cytokine release without cell killing by the HLA-G binding [17].

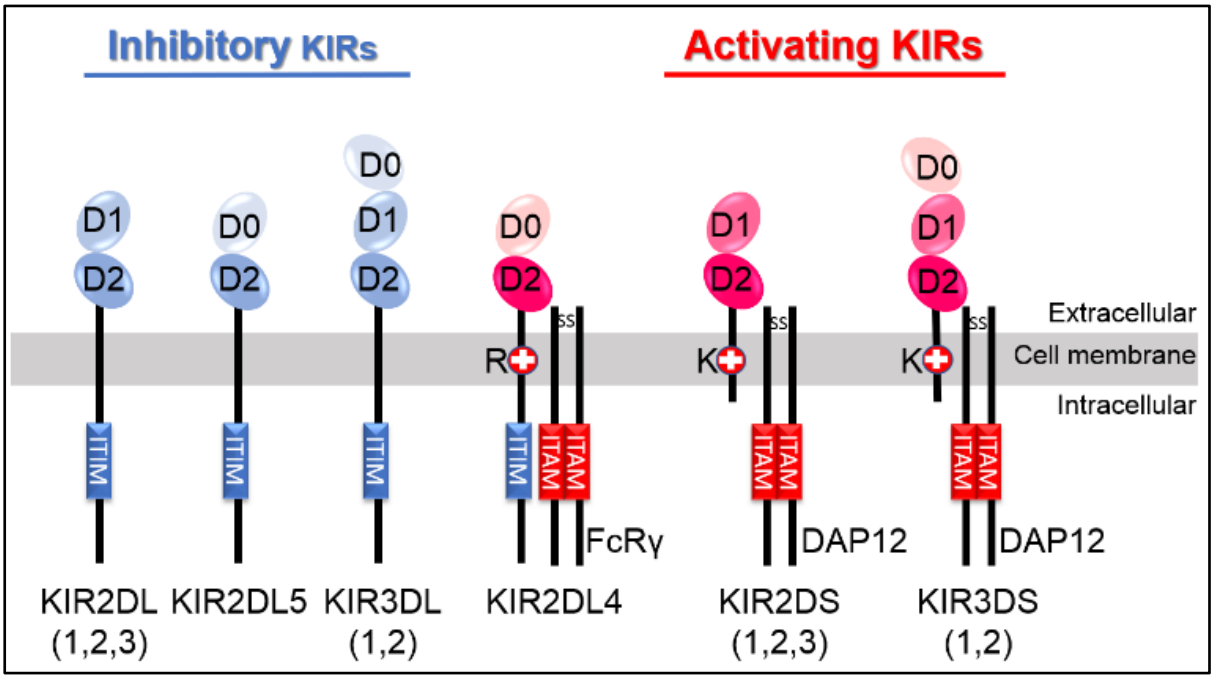

Figure 1: Domain configuration of the KIRs.

3. *KIR* genes and haplotypes

KIR gene family had been mapped on chromosome 19q13.4 called leukocyte receptor complex (LRC) containing lots of genes encoding Ig-like receptors expressed in leukocytes. Thirteen *KIR* genes and two *KIR* pseudogenes, each spanning ~10–16 kb, are tightly arranged in a head-to-tail orientation (Figure 2) [18]. The LRC region has undergone multiple tandem duplications, deletions and insertions so far, which has led to many different haplotypes and highly homologous gene family members. Not all *KIR* genes exist in all individuals due to the presence/absence of gene polymorphism. Therefore, there are highly variable haplotypes which are the combination of *KIR* gene locus. *KIR* locus can be divided into two regions, termed

centromeric (Cen) and telomeric (Tel), by the presence of a recombination hot spot (Figure 2) [19]. Four *KIR* genes are named as the framework genes (i.e., *KIR3DL3*, *KIR3DP1*, *KIR2DL4*, and *KIR3DL2)*, located at the beginning and the ending of these two regions, are generally present in all individuals.

Although there are many haplotypes with different number of *KIR* genes, they have been grouped into two major haplotypes, A and B haplotype (Figure 2). A Haplotype mostly consists of the inhibitory *KIR*s and only one activating *KIR2DS4* that, in some A haplotypes, does not code for a surface receptor [20]. The A haplotypes have a fixed gene content and are composed by Cen-A and Tel-A regions. The other *KIR* haplotypes are collectively named as B haplotypes, and comprise haplotypes carrying Cen-A/Tel-B, Cen-B/Tel-A, and Cen-B/Tel-B combinations (Figure 2) [6].

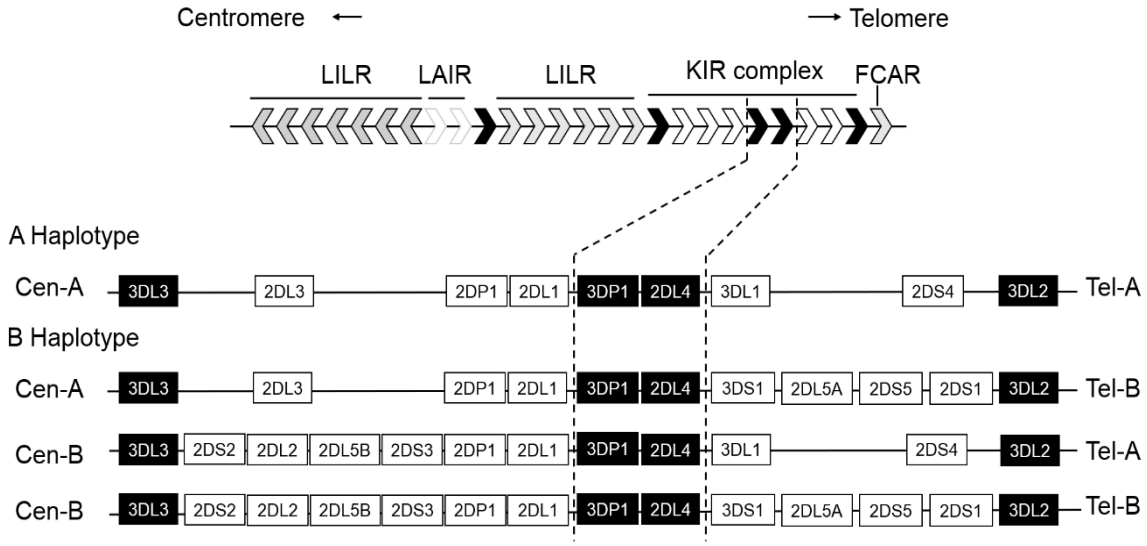

Figure 2: Gene organization of KIR locus.

The nucleotide and amino acid sequences of KIR2Ds are highly homologous and especially in the extracellular domain, there are few differences as shown in Figure 3. This is consistent with the evolution of *KIR* genes by multiple gene duplication. Not only the presence/absence polymorphisms as mentioned above, *KIR* genes have polymorphic residues within the individual genes. Now there are many *KIR* gene alleles including the nonsynonymous substitutions and the polymorphisms within the non-coding regions have been reported at the immuno polymorphism database (IPD)-KIR (https://www.ebi.ac.uk/ipd/kir/).

Figure 3: Alignment of amino acid sequences of KIR2Ds. KIR2DS1 is used as the reference sequence, and dots indicate identity to the reference. D1, D2 mean domain 1, domain 2.

4. Ligands of KIRs

The KIR family predominantly recognizes HLA class I molecules. HLA-C group 1 (HLA-C1) allotypes have an asparagine residue at position 80 (C1: N80) and HLA-C2 allotype have a lysine at position 80 (C2: K80). Some HLA-A alleles and HLA-B allotypes also have either isoleucine (Bw4: I80) or threonine (Bw4: T80). In Table 2, the cellular ligands of KIRs are summarized. KIR2DL1 specifically binds to all HLA-C2 but not to HLA-C1 or any HLA-A or HLA-B allotypes. Although the extracellular domains of some activating KIRs display a high sequence homology with those of its paired inhibitory KIRs (KIR2DS1-KIR2DL1, KIR2DS2-KIR2DL2, L3 and KIR3DS1-KIR3DL1, respectively), the affinities of the activating KIR/HLA class I interactions are weak, and it has been difficult to calculate their binding affinity. For example, KIR2DS1 recognizes HLA-C2 allotypes: HLA-Cw4 (K_d = 30 μM), although with an affinity lower than that of KIR2DL1 (K_d = 7.2 μM) [17]. KIR2DL2 and KIR2DL3 bound HLA-C1 allotypes with sub-μM affinity [21]. Additionally, KIR2DL2/KIR2DL3 showed some binding activity to HLA-C2 but its affinity weaker than the corresponding binding of KIR2DL1 [22]. KIR2DL2 and KIR2DL3 seemed to show a larger peptide dependency on the HLA-C binding than KIR2DL1 [23, 24], and this ability seems to

be particularly relevant for the recognition of the low affinity HLA-C2 allotypes. KIR2DS2 could recognize both HLA-C1 allotypes and HLA-A*11:01 [25, 26]. KIR2DL4 possessing an unusual hybrid structure has been reported to bind HLA-G, a non-classical HLA class I molecule [2]. Functional studies revealed that KIR2DL4 is characterized by a weak inhibitory potential and that its engagement with soluble ligand results in strong cytokine release in the absence of killing [2]. Remarkably, the KIR interaction with HLA class I molecules is highly peptide dependent. That might also suggest the peptides play the key role in the signaling transduction. KIR2DS3, KIR2DS4, and KIR2DS5 have no inhibitory counterparts and KIR2DS3 is expected not to be expressed at the cell surface [27], thus its function and ligand have not been reported. On the contrary, the majority of KIR2DS4 and KIR2DS5 alleles are expected as surface activating receptors [28, 29] and KIR2DS4 binds few HLA-C allotypes carrying either C1 or C2 epitopes as well as HLA-A*11 [30].

KIR3Ds show different preference from KIR2Ds, which mainly recognize HLA-C (Table 2). KIR3DL1 binds not only to HLA-B but also to some HLA-A that carry the Bw4 specificity. KIR3DL2 allotypes bind two HLA-A allotypes (HLA-A*03 and HLA-A*11). Functional analyses revealed that this receptor is characterized by low inhibitory capacity and its ligand interaction is highly dependent on the HLA-A bound peptide. Recently, the ligands of KIR3DS1 have been reported as HLA-B*51, an HLA-B Bw4 I80 allotype, and the open conformer of the non-classical HLA-F molecule [31, 32, 33]

Table 2. HLA class I ligands of KIRs.

Receptors	Cellular ligands
KIR2DL1	HLA-C2 (K80)
KIR2DS1	HLA-C2(K80)
KIR2DL2/L3	HLA-C1 (N80), HLA-B*(46:01 and 73:01), HLA-C2
KIR2DS2	HLA-C1(N80), HLA-A*11:01
KIR2DS3	Unknown
KIR2DL4	HLA-G
KIR2DS4	HLA-C*(02:02, 04:01, 05:01) (K80), HLA-C*(01:02, 14:02, 16:01), HLA-A*11, HLA-F
KIR2DL5	Unknown
KIR2DS5	HLA-C2 (K80)
KIR3DL1	HLA-B Bw4 (T80 and I80); HLA-A*(23:01, 24:02 and 32:01)
KIR3DS1	HLA-F, HLA-B*51
KIR3DL2	HLA-A*03, HLA-A*11; HLA-F
KIR3DL3	Unknown

K80, N80, T80, and I80 mean the responsible amino acid for specific recognition.

5. Crystal structures of KIRs

Consistent with the highly homologous sequences, the reported crystal structures of the ectodomain of KIR2Ds are highly conserved (Figure 4A). The amino acid sequence identity among ectodomain of KIR2Ds is over 90%. Specially, between KIR2DS1 and KIR2DL1, it is 97%. Superimposing the structure of 2DL1(in complex with HLA-Cw4) [34] onto their structures for 192 equivalent Cα atoms gave a root mean square deviation (RMSD) ranging from 0.673 Å for 2DS4 [30], 0.696 Å 2DL2 (in complex with HLA-Cw3) [22] to 1.460 Å for 2DS2 [35] (Figure 4A). As shown in Table 2, most of KIRs recognize HLA class I molecules, especially HLA-C, that would be the reason why the structure and the sequences are highly homologous among KIRs. In contrast to the T cell receptors (TCRs), which recognize a wide area of the bound peptide and its surrounding area (α1 and α2 helices) of the HLA class I, KIR2Ds bind to the C-terminal site of the bound peptide. Thus, the peptide-dependent recognition of KIRs is relatively less specific than that of the TCRs [4].

The complex structures of KIR2Ds with HLA class I molecules also showed the well conserved ligand recognition mechanism (Figure 4B). The V-shaped orientation of two domains has not been largely affected by the ligand binding and the hinge region of KIR2DSs were involved in the HLA class I binding. Comparing the hinge angle of the free KIR2DS2 with that of the complexed KIR2DS2, there is only a small expansion of the hinge angle induced by the binding from 71.2° to 72.4° [25].

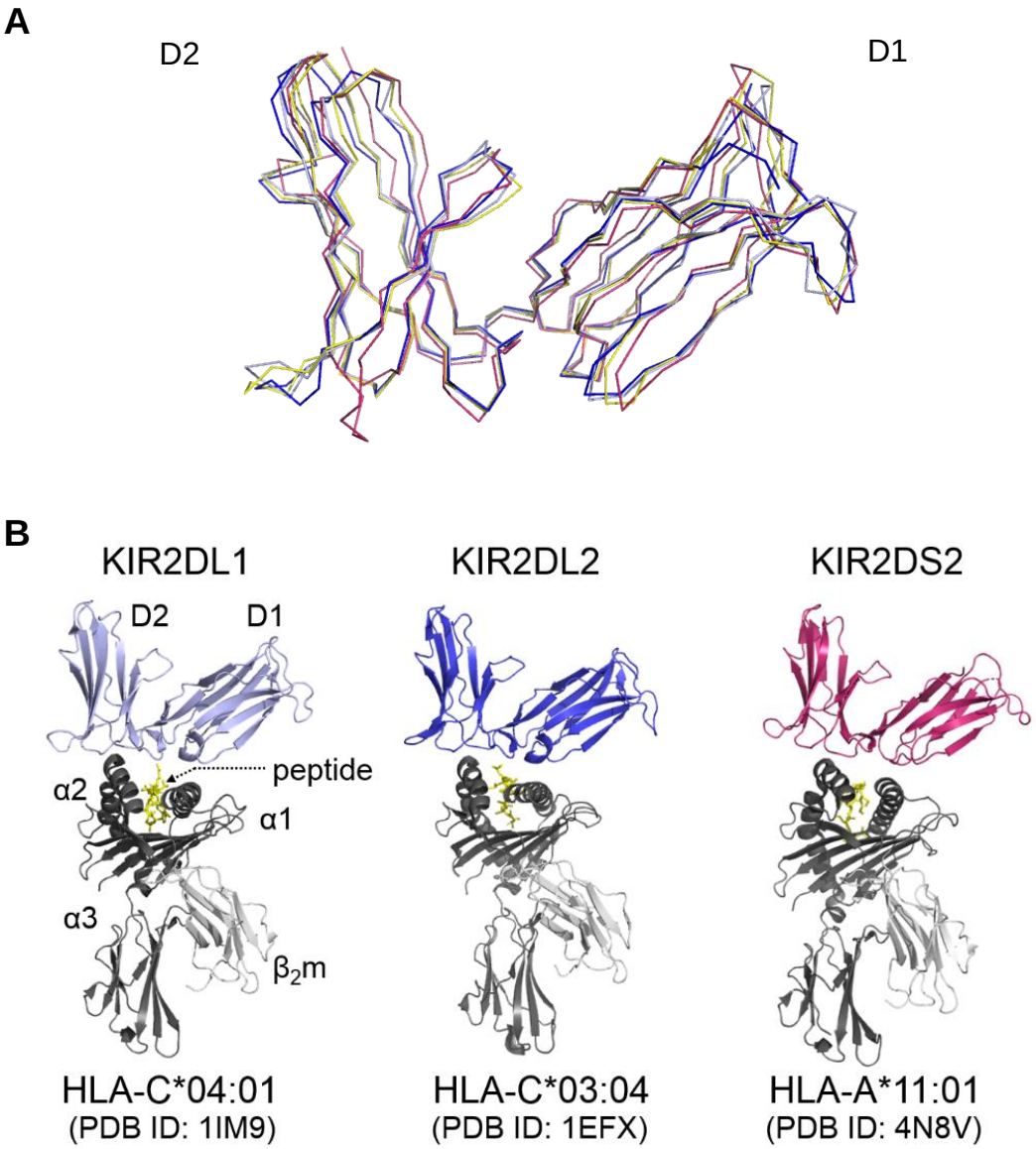

Figure 4: Comparison of the three-dimensional structure of KIR2Ds. (A) The crystal structures of KIR2DS4 (yellow, PDB ID:3H8N), KIR2DL1 (light blue, PDB ID:1IM9), KIR2DL2 (blue, PDB ID: 1EFX) and KIR2DS2 (warmpink, PDB ID:1M4K) are shown in ribbon diagram by PyMOL software. (B) Crystal structures of KIR2D/HLA complex.

The total buried surface area of KIR2DS2 (complex with HLA-A*11:01) between the D1 and D2 domains is 1,020 $Å^2$, which is similar to the reported values for inhibitory KIRs of 2DL1 (1,076 $Å^2$), 2DL3 (1,050 $Å^2$), and 2DL2 (919 $Å^2$). In KIR-HLA complexes, the interface between HLA-A*11:01 and KIR2DS2 is 1,180 $Å^2$, KIR2DL1-HLA-C*04:01 (1,485$Å^2$), KIR2DL2-HLA-C*03:04 (1,562 $Å^2$), and KIR3DL1-B*57:01 (1,740 $Å^2$) [25]. These complex structures revealed that KIR2Ds bind to their HLA ligands, by hydrogen bond and charge complementarity. The mutational studies showed the ligand specificity was strictly determined by the limited different amino acid residues located at the binding region, residue 80 (N or K) of HLA-C and residue 44 (K) of KIR2D [2, 25].

6. KIR and human diseases

The presence/absence of *KIR* gene polymorphisms have been associated with wide range of diseases. To date, *KIR* genes have been showed the statistically significant association with the susceptibility or resistance to viral infections, autoimmune, reproductive, and malignant disorders [1]. *HLA* genes located on chromosome 6 are unlinked to the *KIR* genes located on chromosome 19. Thus, the inheritance and the expression of *HLAs* and *KIRs* are physically independent. However, it has become increasingly clear that the strength of HLA-KIR interactions has functional significance and can influence disease susceptibility [36].

Generally, the combination of *HLA-KIR* genotypes that theoretically lead to lower inhibition and higher activation have been implicated to be beneficial in viral infections such as human immunodeficiency virus (HIV) and hepatitis C virus (HCV), whereas activating genotypes constitute a risk for susceptibility to autoimmunity and perhaps cancers [36]. KIR3DS1-positive NK cell clones were preferentially activated by HIV-1 infected target cells expressing HLA-B Bw4-I80, resulting in lysis of these cells [37]. NK cells from *KIR2DL3/HLA-C1* individuals secreted more IFN-γ at earlier time points after infection and displayed greater degranulation than NK cells from *KIR2DL1/HLA-C2* individuals [38, 39]. The different level of inhibition associated with the presence of the *KIR2DL3/HLA-C1* genotype as compared to *KIR2DL1/HLA-C2* underscore the functional significance of such a difference in response to viral infection [36]. The strong interaction between inhibitory KIR2DL1 and HLA-C2 cripples NK cell activity and prevents the protective NK cell responses against cytomegaloviruses (CMV) [40]. The activating KIR2DS2 might associate the vascular damage/inflammation [41]. $CD4^+CD28^{null}$ T cells, which are expanded in rheumatoid arthritis

(RA) and cause endothelial damage, were found to express KIR2DS2 in the absence of inhibitory KIR2DL2 in this condition [41]. Higher levels of inhibitory KIR-mediated suppression of NK cell activation may also facilitate tumor escape. For example, the *KIR2DL2/2DL3/HLA-C1* genotypes showed significant positive association with melanoma [42] and *KIR3DL1/Bw4 I80* were marginally higher frequencies in the patients with metastatic melanoma [43]. Inhibitory *KIR2DL1/2DL2/2DL3* were also present at significantly higher frequencies in the patients with leukemia [44]. The activating receptors KIR3DS1 and KIR2DS1 were associated with protection in the familial study of Hodgkin's lymphoma [45].

7. Anti-KIR monoclonal antibodies (mAbs)

Recently, KIR family has been targeted as immune checkpoint molecules for clinical application. Lirilumab (IPH2102/BMS-986015, Bristol-Myers Squibb) [46, 47], a first-in-class humanized IgG4 mAb against a common epitope shared by KIR2D, was developed to disrupt mainly the inhibitory KIR (KIR2DL1, KIR2DL2 and KIR2DL3) binding to their ligand, HLA-C molecules. By blocking the inhibitory signals in NK cells, effective killing of tumor target cells had been expected. This antibody has been used for NK cell stimulation in a phase I trial in association with Lenalidomide (a medication used to treat multiple myeloma (MM) and myelodysplastic syndromes (MDS)) to treat MM and acute myeloid leukemia (AML) [47]. However, Lirilumab has failed at a phase 2 clinical trial for AML in 2017. The reason why it failed might be hypothesized that Lirilumab could block the inhibitory KIR2Ds (2DL1/2DL2/2DL3) at the beginning, but also bound with activating KIR2Ds (2DS1/2DS2) possessing the highly conserved amino acid sequence with KIR2DLs. Another humanized antibody, IPH4102 [48], selectively recognizes inhibitory KIR3DL2 which was shown to be highly expressed on cutaneous T cell lymphomas, including mycosis fungoides and Sézary syndrome [49]. In phase 1, IPH4102 has showed encouraging clinical activity in patients with relapsed or refractory cutaneous T-cell lymphoma, particularly those with Sézary syndrome. A multi-cohort, phase 2 trial (TELLOMAK) is ongoing to confirm the activity in patients with Sézary syndrome and explore the role of IPH4102 in other subtypes of T-cell lymphomas that express KIR3DL2 [50].

On the other hand, in the basic research, some KIR molecule-specific monoclonal antibodies are available to use for flow cytometry, immunohistochemistry and western blotting. However, we found a KIR2DS1-specific mAb in commercial showed the cross-binding activity

to other KIR2Ds by surface plasmon resonance (SPR) analysis (unpublished data). Even though there are more mAbs recognizing KIR molecules, such as 143211 (IgG1) specific for KIR2DL1/S5, clone EB6B (IgG1) for KIR2DL1/S1, KIR2DL3*005 and 11PB6 (IgG1) for KIR2DL1/S1, KIR2DL3*005 [6].

8. Novel rat anti-KIR2DS1 specific mAbs

In our laboratory, three novel rat anti-KIR2DS1 specific mAbs (named 1C7, 3E11 and 5B12) have been successfully generated by rat iliac lymph node method. The rats were immunized with the purified KIR2DS1 protein. The enzyme-linked immunosorbent assay (ELISA) clearly showed the specificity of three mAbs (Figure 5). Most of the clones established in this study showed non-specific KIR2D binding like clone 3B4D (Figure 5).

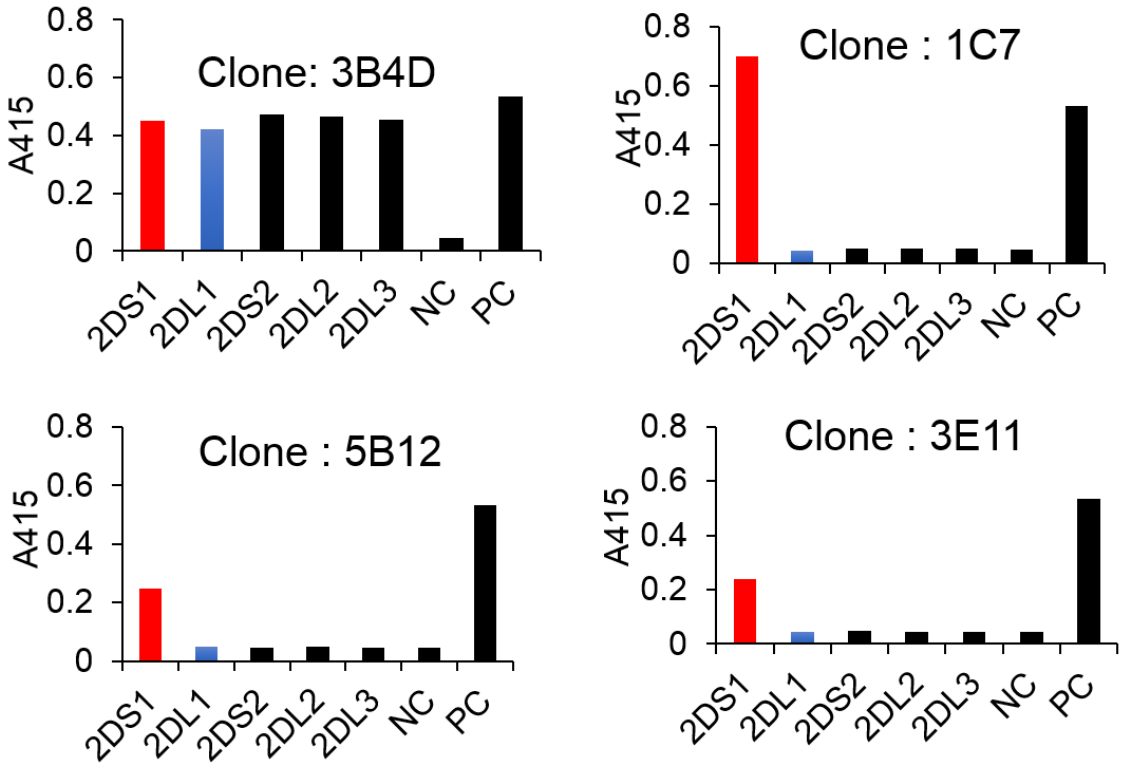

Figure 5: The results of ELSA analysis of rat anti-KIR2DS1 antibodies.
NC: negative control (GIT culture medium). PC: positive control (rat plasma).

By comparing the paired KIR2D, activating KIR2DS1 and inhibitory KIR2DL1, only six amino acid residues are different in the ectodomain as shown in Figure 6. The position of these

six different amino acid residues are shown on the KIR2DL1 crystal structure because the structure of KIR2DS1 has not been elucidated (Figure 7). The surface plasmon resonance (SPR) analysis using KIR2DS1 and KIR2DL1 mutants at these six residues showed that all three mAbs can recognize KIR2DS1 through N163 and only 1C7 clone additionally uses T154 for specific binding (unpublished data). This observation seems to be consistent with the competitive assay of KIR2DS1 binding to HLA-C*0401 molecule and each mAbs. These three mAbs showed partial, not complete, inhibition of HLA-C*0401 binding to KIR2DS1 (unpublished data) probably due to steric hindrance or some overlap of the binding region with mAbs on KIR2DS1 molecule.

The CDR sequences of three clones have been determined (Table 3) (unpublished data). Interestingly, the CDR of light chain was completely identical among them and those of heavy chain also showed high similarity, but there were some differences mainly in the CDR3.

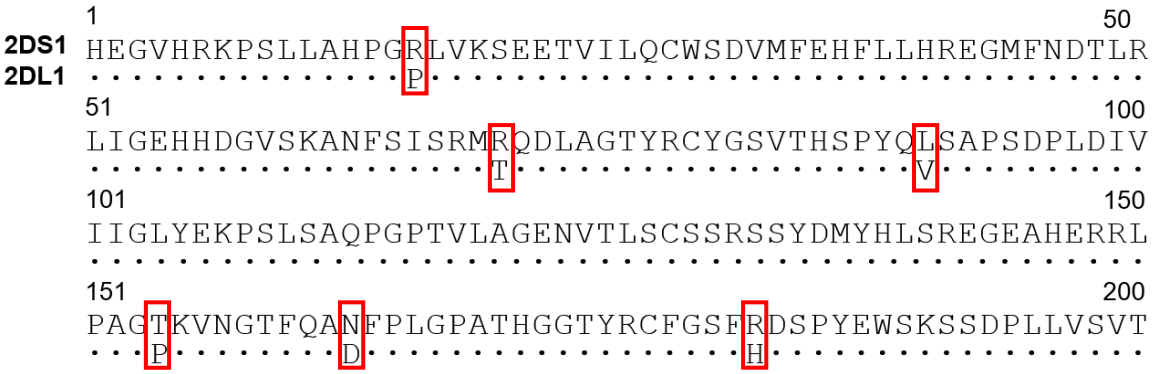

Figure 6: Alignment of amino acid sequences of KIR2DS1 and 2DL1. KIR2DS1 is used as the reference sequence, and dots indicate identity to the reference.

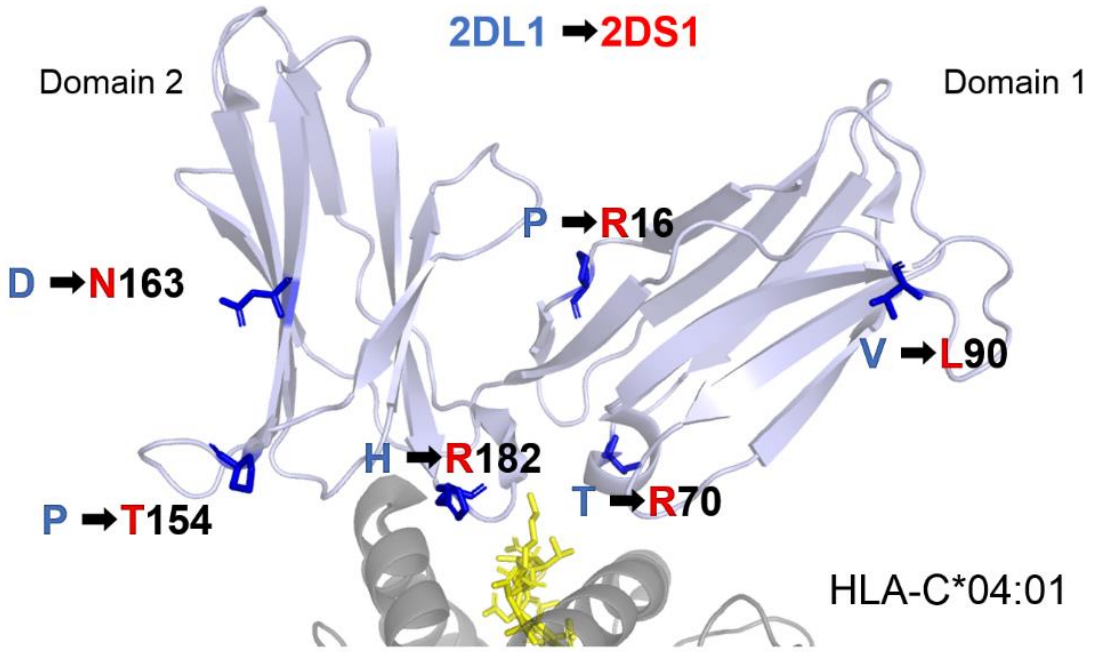

Figure 7. The different amino acid residues between KIR2DS1 and KIR2DL1. The resifues in blue of KIR2DL1 complexed with HLA-C*04:01 (PDB ID: 1IM9) are different in KIR2DS1. The residues of KIR2DS1 are shown in red.

Table 3. CDR sequence comparison of three antibodies.

		CDR1	CDR2	CDR3
VL	1C7	KASQNVGSNVD	KASNRYT	MQSNTNPLT
	5B12	·····G·····	·····	·····
	3E11	·····	·····	·····
VH	1C7	GFSLSTY**S**MGVS	SIWWNGNTYNNPSLKS	T**E--IIRGRN**YYVMDA
	5B12	·····**G**····	·····	·**LITIAAISH**·····
	3E11	·····**G**····	·····	·**LITITPF--**·····

CDR: complementarity-determining region, VH: variable heavy chain; VL: variable light chain

Objectives

These specific mAbs against KIR2DS1 are expected to be used for the basic research to clarify the expression properties of KIR2DS1 in the NK cell-related immune disorders, and to be developed as candidates for therapeutic antibody drugs as well. To understand the molecular recognition of KIR2DS1 by novel specific antibodies, I clarified the crystal structure of KIR2DS1 antigen and compare with those of other KIR2Ds. Next, I determined the binding properties of novel antibodies to KIR2DS1, and finally revealed the crystal structure of the Fab fragment of KIR2DS1-specific antibody.

Materials and methods

1. Preparation of recombinant KIR2DS1 protein

The gene encoding human KIR2DS1 (residues 1-200) was cloned into the plasmid vector pGMT7 for the expression in *E.coli*. The recombinant protein of KIR2DS1 was prepared as previously described for LILRB1 and LILRB2 [51]. KIR2DS1 was expressed as inclusion bodies in BL21(DE3)pLysS (Novagen, now Merck, Darmstadt, Germany). Briefly, the BL21(DE3)pLysS competent cells stored in the -80°C was thawed on ice and was transformed by the plasmid of KIR2DS1-pGMT7 with heat-shocked at 42°C for 40 seconds. After 2 minutes incubation on ice, these cells were recovered in 2×YT culture medium at 37°C for 1 hour and were plated on the LB agar plate with 100 μg/mL ampicillin and incubated overnight at 37°C. On the second day, some colonies were picked from the plate and precultured in the 5 ml 2×YT culture medium with 100 μg/mL ampicillin by shaking at 150 rpm at 37°C for 5 hours. Then the 5 ml culture was transferred to 1 L of sterilized culture medium with 100 μg/mL ampicillin was inoculated by the grown cultured medium for large scale culture, and was shaking at 150 rpm at 37°C. Then the expression of KIR2DS1 was induced by adding 1 mM isopropyl β-D-1-thiogalactoppyranoside (IPTG) when the OD_{600} has reached 0.4-0.6. After 4 hours shaking at 37°C, the *E.coli* cells were harvested by centrifugation at 5000 rpm at 4°C for 10 minutes. To prepare the inclusion bodies of KIR2DS1, the cell pellet was resuspended with 40 mL resuspension buffer (50 mM Tris-HCl, pH 8.0 and 150 mM NaCl), and sonicated by SONIFIER 250 Advanced (BRANSON, Connecticut, US). After the disintegration of the cells, the inclusion bodies were harvested and washed 3 times each by Triton wash buffer (suspension buffer containing 0.5% Triton X-100) and resuspension buffer. The inclusion bodies were solubilized in 6 M guanidine hydrochloride (Gu-HCl) buffer (6 M Gu-HCl, 50 mM Tris-HCl, pH 8.0 and 10 mM EDTA).

Before the refolding of KIR2DS1 recombinant proteins, the solubilized proteins were reduced by incubation with 2 mM DTT at room temperature for 1 hour. The denatured KIR2DS1 protein was refolded by the gradual dilution method using the refolding buffer (1 M L-Arginine hydrochloride, 100 mM Tris-HCl pH 8.0, 2 mM EDTA, 3.73 mM cystamine dihydrochloride and 6.34 mM cysteamine hydrochloride). The solution of KIR2DS1 protein (468 μM) was diluted to reach the final protein concentration of 1-2 μM. The 1 L of the refolding buffer containing KIR2DS1 was constantly stirred at 4°C for 3 days. The refolded protein solution was concentrated to about 20 mL by using an ultrafiltration system, Vivaflow 50 (MWCO 10,000 Da) (Sartorius, Goettingen, Germany).

The concentrated protein solution was filtered with a membrane filter (0.22 μm pore size) and was applied to HiLoad 26/60 Superdex75 pg column (GE Healthcare, Buckinghamshire, UK) for size exchange chromatography (SEC) using AKTA Purifier system (GE Healthcare). The target fractions eluted at the estimated position were collected and checked by the sodium dodecyl sulfate-polyacrylamide gel electrophoresis (SDS-PAGE) and Coomassie brilliant blue (CBB) staining to be eluted as the refolded proteins. The peak fractions containing refolded KIR2DS1peoteins were buffer-exchanged to 20 mM Tris-HCl, pH 8.0 (A buffer of AEC) and applied to RESOURCE Q 1mL column (GE Healthcare) for anion exchange chromatography (AEC). The KIR2DS1 proteins were eluted with 40 column volume (CV) linear gradient of 0-0.5 M NaCl in A buffer using AKTA Purifier system (GE Healthcare).

The proteins in the eluted fractions were separated by SDS-PAGE. The proteins mixed with sample buffer (125 mM Tris·HCl pH 6.5, 25% glycerol, 5% SDS, 0.25% bromophenol blue with [reducing condition]/without [non-reducing condition] 5% 2-mercaptoethanol) were applied to 15% acrylamide gels. In the case of reducing condition, the samples were boiled at 95°C for 5-10 min. The loaded proteins were separated in the gel with running buffer (25 mM Tris, 190 mM glycine and 0.1% SDS) by electrophoresis (30 mA 60-70 min), and then proteins were visualized by CBB or silver staining to analyze the final purity.

The KIR2DS1 with the C-terminal biotin ligase (BirA) recognition sequence (GSLHHILDAQKMVWNHR) were prepared same as KIR2DS1 protein. After purification, KIR2DS1 was enzymatically biotinylated with BirA in 50 mM D-biotin pH 8.3, 10 mM ATP, 10 mM magnesium acetate. After biotinylation, KIR2DS1s were separated from the reaction mixture by gel filtration (Column: Superdex 75 10/300 (GE Healthcare)). The biotinylated KIR2DS1s were used for the immobilization on the CAPture chip for SPR analysis.

2. Purification of monoclonal antibodies and their Fab fragments

Three hybridoma cell lines for anti-KIR2DS1 specific monoclonal antibodies (1C7, 5B12, and 3E11) were cultured in RPMI 1640 complete medium with 10% fetal bovine serum (FBS) for 3-4 days at 37°C with 5% CO_2. When the culture dishes reach ~80% confluent, the cells were centrifuged at 300×g for 5 minutes. The cell pellets were resuspended by RMPI 1640 complete medium with 2% FBS and were cultured for about 2 weeks for antibody production at 37°C with 5% CO_2. The 2% FBS was determined by the experiment that comparing the yield that culture with 0-3% FBS. The 2% FBS had the highest yield of producing antibodies.

Then the medium was transferred to the 50 ml Falcon tubes. After taking the balance, the tubes were centrifuged at 9000×*g* for 5 minutes by Kubota High Speed Refrigerated Centrifuge Model 6000. Then the supernatant was filtered with the membrane filter (pore size 0.22 μm) to remove the cellular debris and applied to Protein G Sepharose 4 Fast Flow (GE Healthcare) for affinity chromatography purification. 0.5 ml protein G resin was added into 50 mL culture supernatant and rotated by laboratory sample rotator at 4°C for 2 hours, and then purified using Econo-Pac® Chromatography Column (BioRad). The resin was washed by 20 mM Na-Pi pH 7.0 and eluted by 0.1 M glycine-HCl (pH 3.0, pH 2.5 and pH 2.0). Every 1 mL eluted fractions were neutralized by 1 M Tris-HCl pH 9.0 (20 μL to pH 3.0, 70 μL to pH 2.5 and 110 μL to pH 2.0, respectively). The purity of the eluted mAb fractions was analyzed by SDS-PAGE (15% acryl amide gel) and CBB staining. All the elution samples were collected and apply to the next step.

For the papain digestion of mAbs, the eluted mAb proteins were buffer exchanged to the sample buffer: 20 mM sodium phosphate, 10 mM EDTA; pH 7.0 by dialysis using Spectra/Por 7 Pretreated Regenerated Cellulose (Spectrum Laboratories) at 4°C overnight. The mAbs proteins in the sample buffer were digested by immobilized papain (Thermo Scientific™). 0.5 mL of the purified mAb protein solution was mixed with 0.5 mL of digestion buffer (sample buffer with 20 mM cysteine·HCl), and applied to 0.5 mL immobilized papain resuspended by 0.5 ml digestion buffer in the 1.5 mL tube. The sample was incubated with shaking at 150 rpm at 37°C overnight. After adding 1 mL of 10 mM Tris-HCl, pH 7.5, the immobilized papain was separated by centrifugation. The supernatant which contains the digested Fab and Fc fragments were collected and buffer-exchanged to 5 mM Tris-HCl, pH 8.0, 35 mM NaCl by dialysis at 4°C overnight. The samples were purified by anion exchange chromatography (AEC) with Hi-trap Q HP 1mL column (GE Healthcare) using 5 mM Tris-HCl, pH 8.0 as the binding buffer and 5 mM Tris-HCl, pH 8.0, 1 M NaCl as the elution buffer. The Fab fragments were eluted with 35 CV linear gradient of 0-0.4 M NaCl using AKTA Purifier system (GE Healthcare). The final purity was analyzed by SDS-PAGE and CBB staining.

3. Surface plasmon resonance (SPR) analyses

SPR analyses were performed using BIAcore3000 (GE Healthcare). The C-tereminal biotinylated KIR2DS1 protein, were immobilized on a Sensor chip CAP of Biotin CAPture kit (GE Healthcare) through the captured streptavidin proteins (SA) (about 1000 response unit

(RU) for kinetic analysis and about 1000 RU for Equilibrium (Eq)-binding analysis) (Figure 8). The SA-captured flow cell with no ligand was used as a negative control flow cell.

For kinetic analysis using the mAbs, the purified antibody protein in the HBS-EP (0.01 M HEPES pH 7.4, 0.15 M NaCl, 3 mM EDTA, 0.005% v/v Surfactant P20) buffer (GE Healthcare) was independently injected over each flow path at 25 μL/min. The specific binding responses were calculated by subtracting a response derived from the SA-immobilized control flow path. For the mAb, the kinetic parameters were calculated using a local fitting by bivalent binding model (A+ B ⇔ AB, AB+B ⇔ AB_2) using BIAevaluation Software 4.1.1(GE Healthcare). To calculate the apparent dissociation constants (K_d), the local fitting was performed by 1:1 Langmuir binding model (A+ B ⇔ AB).

To consider the avidity effects of the mAbs binding to KIR2DS1, binding analysis using the monovalent Fab fragments were performed by using the Equilibrium (Eq)-binding analysis. The Fab fragment solutions were injected over the sensor chip at 5 μL/min and the specific binding response units were calculated by subtracting the response unit of the SA-immobilized control flow path. The monovalent binding fitting model was applied to calculate the dissociation constant (K_d) using BIAevaluation Software 4.1.1 (GE Healthcare). The definition of parameters used in this study are described in Table 4.

Thermodynamic analysis was performed by Eq-binding SPR analyses using Fab fragments at six different temperature points (10°C, 12°C, 15°C, 20°C, 25°C and 30°C). Using the dissociation constant (K_d) obtained at each temperature, the standard state Gibbs energy change upon binding was obtained from equation (a):

$$\Delta G = RT \ln K_d \quad \text{(a)}$$

where R is the gas constant (R = 8.314 J / mol·K). ΔG of each data set were plotted against the temperatures, and the fitted with the non-linear van't Hoff equation using Origin software 2017 version (LightStone) (equation (b)):

$$\Delta G = \Delta H - T\Delta S + \Delta C_p(T\text{-}298.15) - \Delta C_p T \ln(T/298.15) \quad \text{(b)}$$

where ΔH and ΔS are the binding enthalpy and entropy at 298.15 K, respectively, and ΔC_p is the heat capacity, which is assumed to be temperature independent.

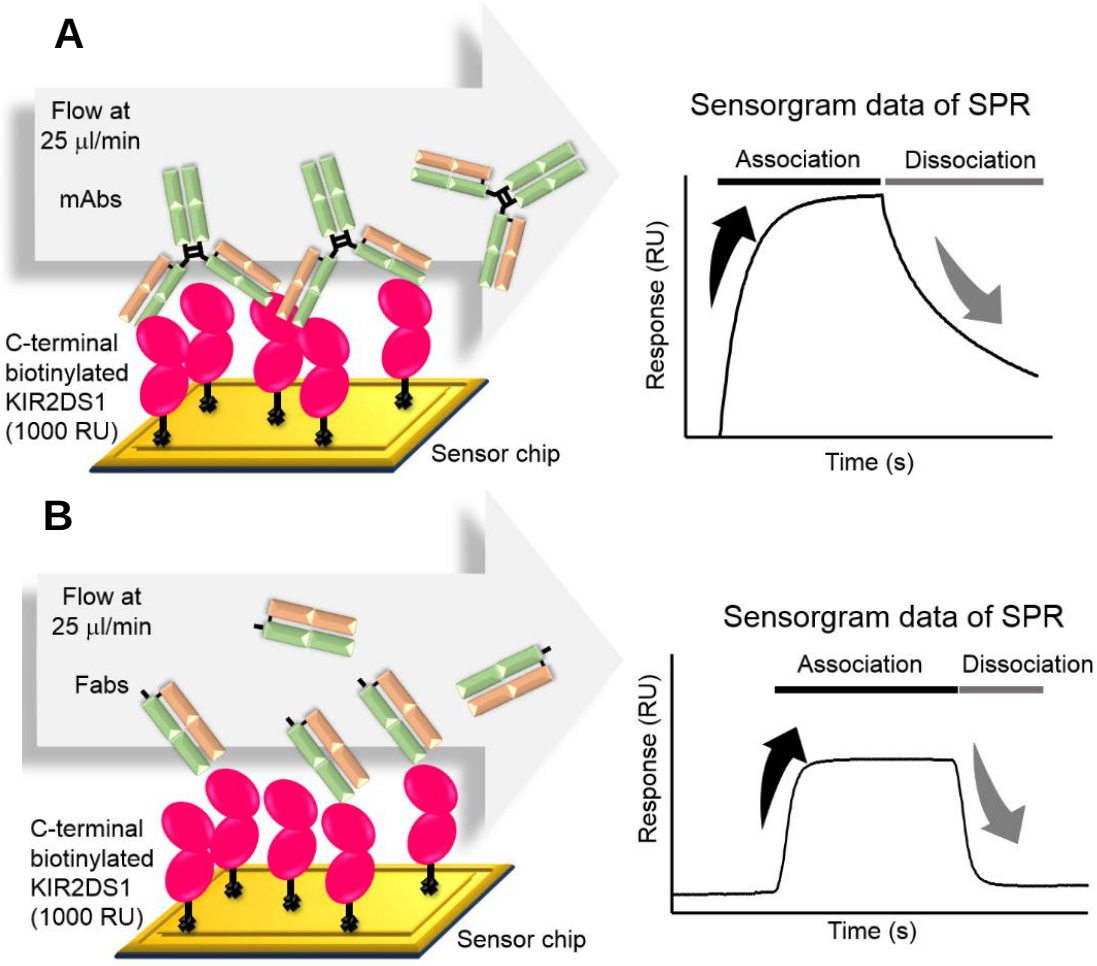

Figure 8: SPR analyses used in this study. (A) Model of kinetic analysis of mAbs–KIR2DS1 binding by SPR. The C-terminal biotinylated KIR2DS1 was immobilized on the sensor chip, and each mAb was injected over the KIR2DS1. When the mAbs get associated with KIR2DS1, the response signal will increase, and if the mAbs dissociate from KIR2DS1, the response will decrease. (B) Model of equilibrium-binding analysis of Fabs–KIR2DS1 by SPR. Each Fab fragment was injected over the immobilized KIR2DS1. Fab has one ligand-binding region, thus the monovalent binding sensorgram is expected like this with a faster dissociation rate than the bivalent mAb binding.

Table 4. Definition of parameters in SPR analysis.

Parameter		Description
1:1 Langmuir binding model	k_{on}	Association rate constant for A+B => AB (1/Ms)
	k_{off}	Dissociation rate constant for AB => A+B (1/s)
	K_A	Equilibrium association constant. k_{on} / k_{off} (1/M)
	K_D	Equilibrium dissociation constant. k_{off}/ k_{on} (M)
Bivalent binding model	k_{on}^1	Association rate constant for A+B => AB (1/Ms)
	k_{off}^1	Dissociation rate constant for AB => A+B (1/s)
	k_{on}^2	Association rate constant for AB+B => AB_2 (1/RUs)
	k_{off}^2	Dissociation rate constant for AB_2 => AB+B (1/s).
Both models	R_{max}	Maximum analyte binding capacity
	Chi2	Standard statistical measure of the closeness of fit

4. Crystallization and structure determination of KIR2DS1

The purified KIR2DS1 proteins in Tris-HCl buffer pH 8.0 with NaCl by AEC were concentrated to 7.8 mg/mL by using Amicon Ultra filter (MWCO; 10K) (Millipore). Initial crystallization screening was performed with commercially available kits, Classic II suit kit (Qiagen) by the sitting-drop vapor-diffusion method. Briefly, 200 nL of the protein solution was mixed with an equal volume of reservoir solution by using mosquito crystal Nanolitre Protein Crystallization robot. Crystals of KIR2DS1 were obtained with a reservoir solution containing 0.2 M ammonium sulfate, 0.1 M HEPES pH 7.5, 25% (w/v) PEG 3350 at 20°C. For data collection, the crystals of KIR2DS1 were soaked into a cryoprotectant solution (the reservoir solution containing 25% (v/v) ethylene glycol) and then flash-cooled in a stream of nitrogen at 100 K. X-ray diffraction data for KIR2DS1 were collected on the beamline X06SA(PXI) of Swiss Light Source (Switzerland).

The structure was determined by the molecular replacement method with the program *Molrep* in the *CCP4* suite, using the structure of KIR2DL1 (PDB ID: 1IM9) as a search model. Rotation and translation functions were calculated using data from 44.4 to 3.9 Å resolution. The structures were modified manually with *Coot* and refined with *Refmac5* and *phenix.refine*. Structures were displayed using PyMOL (PyMOL Molecular Graphics System).

5. Crystallization and structure determination of 1C7 Fab

The purified 1C7 Fab proteins in Tris-HCl buffer, pH 8.0 were concentrated to 7.5 mg/mL, using an Amicon Ultra filter (MWCO; 30K) (Milipore), and subsequently used for the initial screening of crystallization using PEGs Suit and PEGs II Suit kits (Qiagen) by the sitting-drop vapor-diffusion method using a mosquito robot. Briefly, 200 nL of the protein solution was mixed with an equal volume of reservoir solution. Crystals of KIR2DS1 were obtained in the reservoir solution containing 0.1M Tris pH 8.5 30% (w/v) PEG1000 and incubated at 20°C. For data collection, the crystals of 1C7 Fab were soaked into a cryoprotectant solution containing 20% (v/v) glycerol and then flash-cooled in a stream of nitrogen at 100 K. X-ray diffraction data for 1C7 Fab were collected on the beamline BL17A of the Photon Factory (Tsukuba, Japan).

The data set for 1C7 Fab was processed using the HKL-2000 program suite. The structure was determined by the molecular replacement method with the program *Molrep* in the *CCP4* suite, using the structure of heavy chain: Cationic Cyclization Antibody 4C6 (PDB ID: 1NCW) and light chain: murine IgG2a A27D7 (PDB ID: 4M1G) as search models. Rotation and translation functions were calculated using data from 46.5 to 2.0 Å resolution. The structures were modified manually with *Coot* and refined with *Refmac5* and *phenix.refine*. Structures were displayed using PyMOL (PyMOL Molecular Graphics System).

Results

1. Structural analysis of KIR2DS1

1-1. Preparation of KIR2DS1 recombinant protein

The recombinant KIR2DS1 protein was produced in *E.coli* as inclusion bodies and was refolded by the dilution method as described in Materials and methods. The refolded protein was purified from the unfolded aggregates by size exclusion chromatography (SEC) and the collected fractions were analyzed by SDS-PAGE to confirm the purity. The refolded KIR2DS1 was eluted as a major peak by SEC, and the fractions shown by the black arrow were collected as properly refolded KIR2DS1 (Figure 9A). The SDS-PAGE analysis under reduced condition revealed a single major band for KIR2DS1 (theoretical molecular weight = 23.5 kDa (Figure 9B).

The collected KIR2DS1 protein solution was dialyzed and buffer-exchanged to the wash buffer of anion exchange chromatography (AEC) for the second chromatography. KIR2DS1 was eluted as a major peak with a shoulder, thus the main peak without shoulder fraction as described by a black arrow was collected and used for the crystallization (Figure 9C). The purity was examined by SDS-PAGE under reducing condition (Figure 9D).

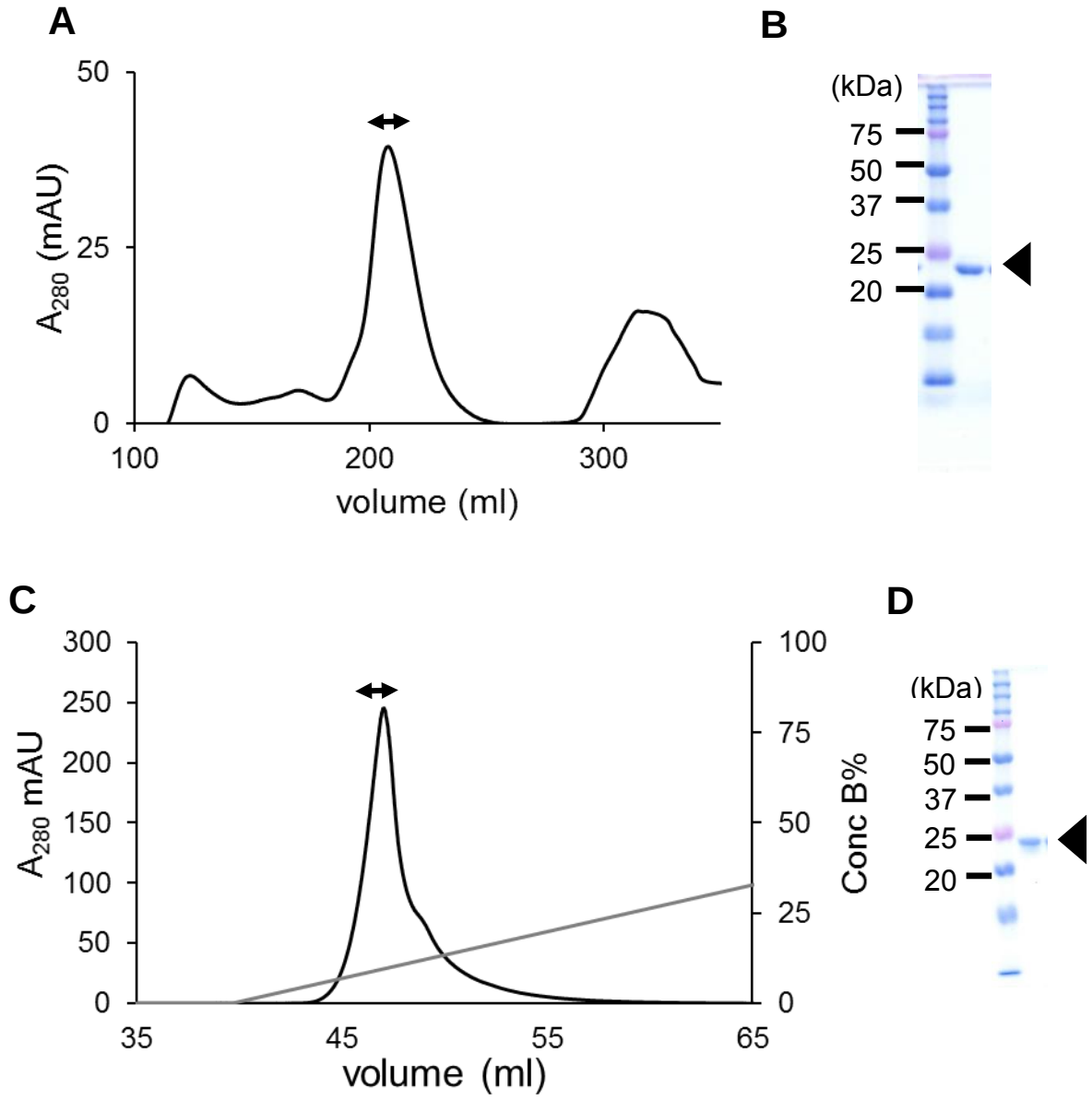

Figure 9: The purification of KIR2DS1 protein. (A) SEC of KIR2DS1 protein with Hiload 26/60 Superdex 75 column and 20 mM Tris-HCl pH 8.0; 100 mM NaCl buffer. Eluted KIR2DS1 protein was indicated by the peaks under the black arrows. (B) SDS-PAGE of purified KIR2DS1 by SEC. The gel contains 15% acrylamide and was stained by CBB. The sample was reduced by 5% 2-mercaptoethanol. (C) AEC of KIR2DS1 protein after SEC (0-50%B/40 column volume). (D) SDS-PAGE of purified KIR2DS1 by AEC.

1-2. The crystallization and structural determination of KIR2DS1

To understand the molecular recognition of KIR2DS1 by the novel antibodies, the crystallization of KIR2DS1 was performed. The purified KIR2DS1 recombinant protein was concentrated by ultra-filtration to 7.8 mg/mL. Crystals of KIR2DS1 was successfully obtained in the reservoir buffer: 0.2 M ammonium sulfate, 0.1 M HEPES pH 7.5, 25% (w/v) PEG 3350 at 20°C (Figure 10A), and the X-ray diffraction data set was collected on the beamline X06SA(PXI) at the Swiss Light Source.

The crystal structure of KIR2DS1 was determined at the resolution of 3.92 Å by the molecular replacement method using the KIR2DL1 structure (PDB ID: 1IM9) as a search model (Figure 10B). The data collection and processing statistics are summarized in Table 5. The model of KIR2DS1 was refined until the final value of R_{work} and R_{free} factors were determined as 36.64% and 38.99% converged using refinement programs.

The overall structure of KIR2DS1 looks similar to those of other KIR2Ds consistent with the highly conserved their amino acid sequences. Especially, the main chain structure of KIR2DS1 was well superimposed by that of KIR2DL1 which has only six different amino acid residues from KIR2DS1 (Figure 10C). Unfortunately, the orientation of side chains could not be clearly located in the low-resolution electron density map (Figure 10B), thus only the main chain structure of KIR2DS1 will be discussed in this study. The amino acid residues discriminated by the KIR2DS1-specific mAbs, N163 and T154, may not cause apparent structural change as shown in Figure 10D.

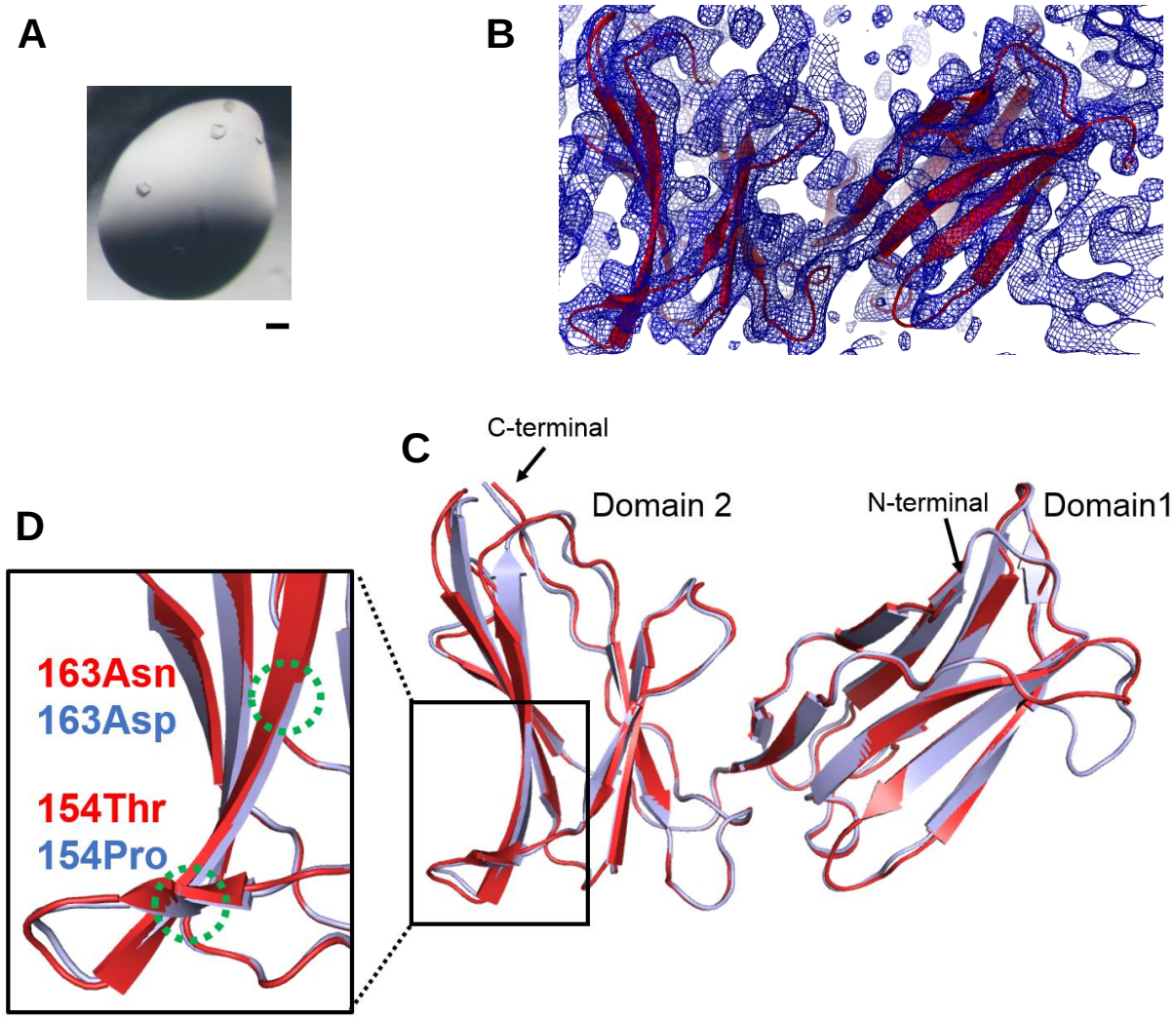

Figure 10: Crystallization of KIR2DS1. (A) The picture of KIR2DS1 crystals. The black bar indicates 100 µm. (B) Stereo view of the $2F_o–F_c$ map around the KIR2DS1 chain A. KIR2DS1 structure was shown in red cartoon. The $2F_o–F_c$ maps were contoured at 1.0 σ. (C) Comparing of the structures of KIR2DS1 and KIR2DL1 in cartoon model. KIR2DS1 was shown in red, KIR2DL1 was shown in blue. Root Mean Square Deviation (RMSD) value is 0.469 Å. (D) The Zoomed-in view of the structure around the residues at 163 and 154. The amino acid residues at 163 and 154 were shown in the dashed green circles.

Table 5. Data collection and refinement statistics

Data collection	**KIR2DS1**
wavelength (Å)	1.00
resolution (Å)	3.92
space group	$I\,2_1\,3$
unit-cell parameters (Å)	a=b=c=177.771
multiplicity	2.0 (2.0)
completeness (%)	99.82 (100.00)
$\langle I/\sigma(I)\rangle$	24.66 (7.89)
R_{sym}	0.3232 (0.1349)
unique reflections	8551 (852)
Refinement	
resolution (Å)	3.92
R_{work}/R_{free}	0.3664/0.3899
Number of atoms	2964
macromolecules	2964
RMSD	
Bond length (Å)	0.003
Bond angle (°)	0.59
Ramachandran (%)	
favored	93.09
allowed	6.65
outliers	0.27
Mean B-factor (Å^2)	105.24
macromolecules	105.24

2. The binding properties of three clones with KIR2DS1 protein

2-1 The preparation of anti-KIR2DS1 specific mAbs and their Fab fragments

The novel anti-KIR2DS1 specific mAbs were produced by the established hybridoma cells as described in Materials and Methods. The mAbs were purified by the protein G affinity chromatography from the culture supernatants. The purity of mAbs were examined by SDS-PAGE under reducing conditions with CBB staining (Figure 11).

Furthermore, the Fab fragments of three mAbs were prepared for SPR analysis and structural analysis. The purified mAbs were digested by papain at 37°C overnights. The digested Fab and Fc fragments were separated by SDS-PAGE (Figure 12A, 13A and 14A). The Fab fragments were eluted in the 1st peak fraction by AEC (Figure 12B, 13B and 14B). The SDS-PAGE showed that the 2nd and the 3rd peaks contains Fc fragments (Figure 12C, 13C and 14C).

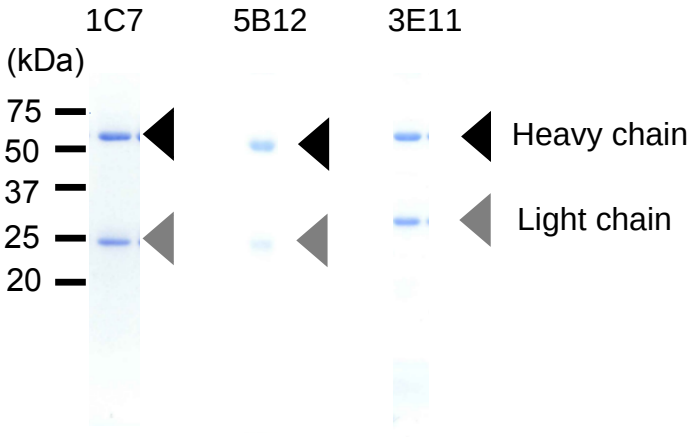

Figure 11: **SDS-PAGE of purified mAbs by protein G purification.** The gel contains 15% acrylamide and was stained by CBB. The sample was reduced by 5% 2-mercaptoethanol.

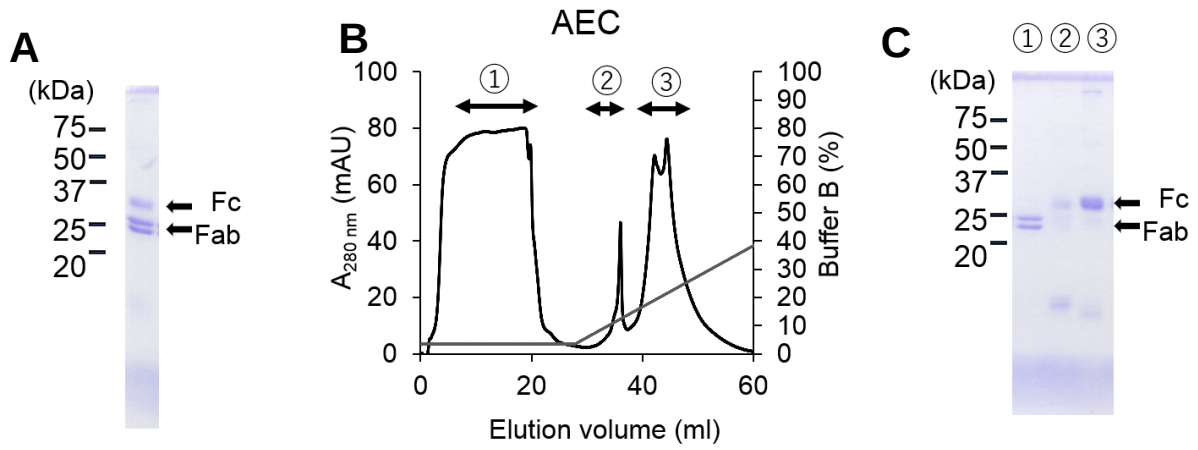

Figure 12: Purification of 1C7 Fab. (**A**) SDS-PAGE of 1C7 Fc and Fab fragments after papain digestion. The gel contains 15% acrylamide and was stained by CBB. The sample was reduced by 5% 2-mercaptoethanol. (**B**) The chromatogram of AEC. The eluted proteins were collected independently under the black arrow number 1, 2 and 3. (**C**) SDS-PAGE of eluted proteins by AEC.

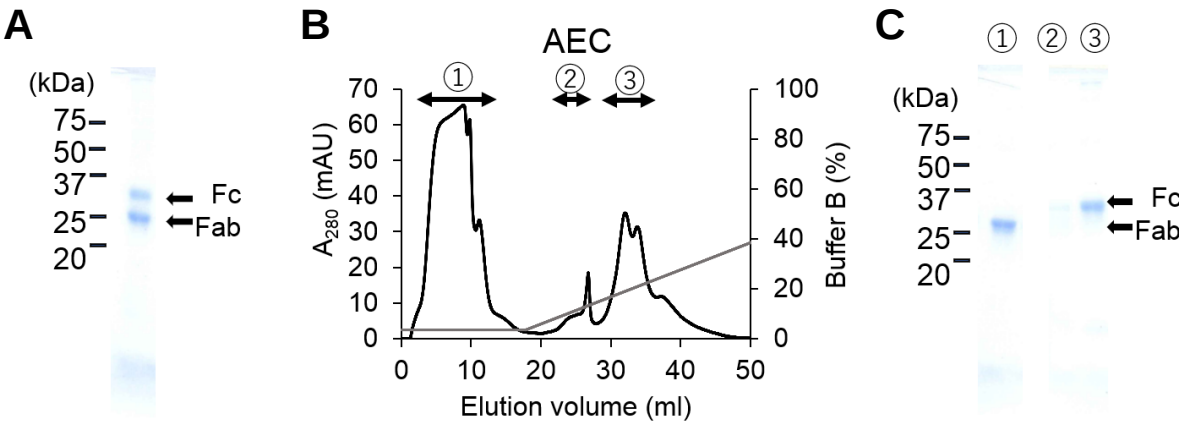

Figure 13: Purification of 5B12 Fab. (**A**) SDS-PAGE of 5B12 Fc and Fab fragments after papain digestion. The gel contains 15% acrylamide and was stained by CBB. The sample was reduced by 5% 2-mercaptoethanol. (**B**) The chromatogram of AEC. The eluted proteins were collected independently under the black arrow number 1, 2 and 3. (**C**) SDS-PAGE of eluted proteins by AEC.

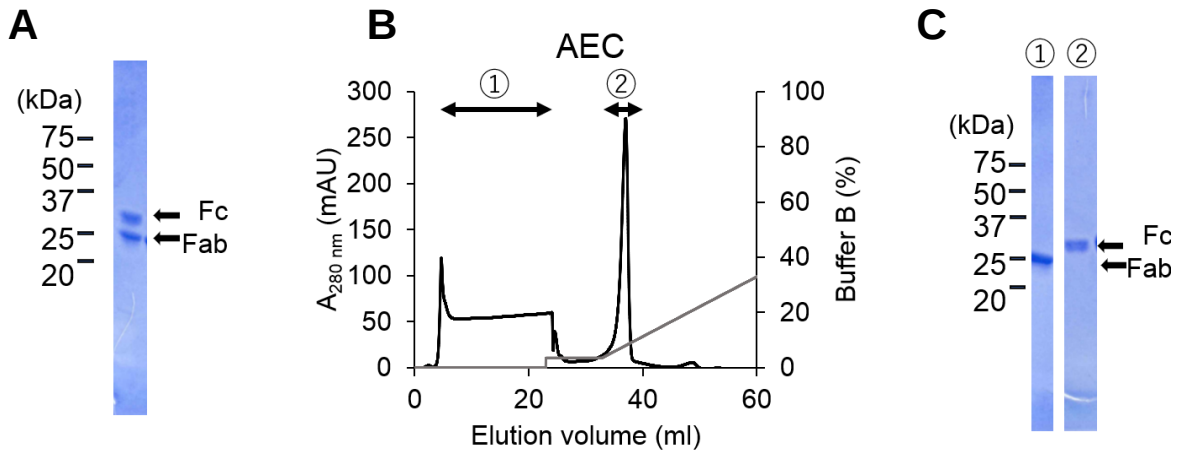

Figure 14: Purification of 3E11 Fab. (**A**) SDS-PAGE of 3E11 Fc and Fab fragments after papain digestion. The gel contains 15% acrylamide and was stained by CBB. The sample was reduced by 5% 2-mercaptoethanol. (**B**) The chromatogram of AEC. The eluted proteins were collected independently under the black arrow number 1 and 2. (**C**) SDS-PAGE of eluted proteins by AEC.

2-2. The kinetic analysis of mAbs-KIR2DS1 using SPR

To verify and compare the binding affinity of three mAbs to KIR2DS1 protein, SPR analysis was performed at 25°C. The KIR2DS1 protein was prepared as a C-terminal biotinylated protein to maintain the orientation and the molecular shape of immobilized KIR2DS1 as it was in the cellular membrane. Because all mAbs showed the binding to the immobilized KIR2DS1 with slow dissociation in the preliminary experiment, kinetic analysis was performed to calculate their binding affinities. Each mAb (1C7, 3E11 and 5B12) was injected over the immobilized KIR2DS1, and representative data were shown in Figure 15. 1C7 mAb showed the slowest dissociation rate compared with others (Figure 15). Because mAbs have two arms for antigen-specific binding, the kinetic analysis of mAbs binding to KIR2DS1 well fitted with the bivalent analyte model.

To know the apparent binding affinity of mAbs to KIR2DS1, the 1:1 Langmuir binding model was applied to the mAbs-KIR2DS1 binding sensorgram. The fitting data and the kinetic parameters calculated by the 1:1 Langmuir binding model revealed the apparent K_D values of mAb 1C7, 5B12, 3E11 calculated by the 1:1 Langmuir binding model were 2.5-3.3 nM, 15-44 nM, and 22-234 nM, respectively. Thus, 1C7 mAb showed the highest apparent affinity to KIR2DS1.

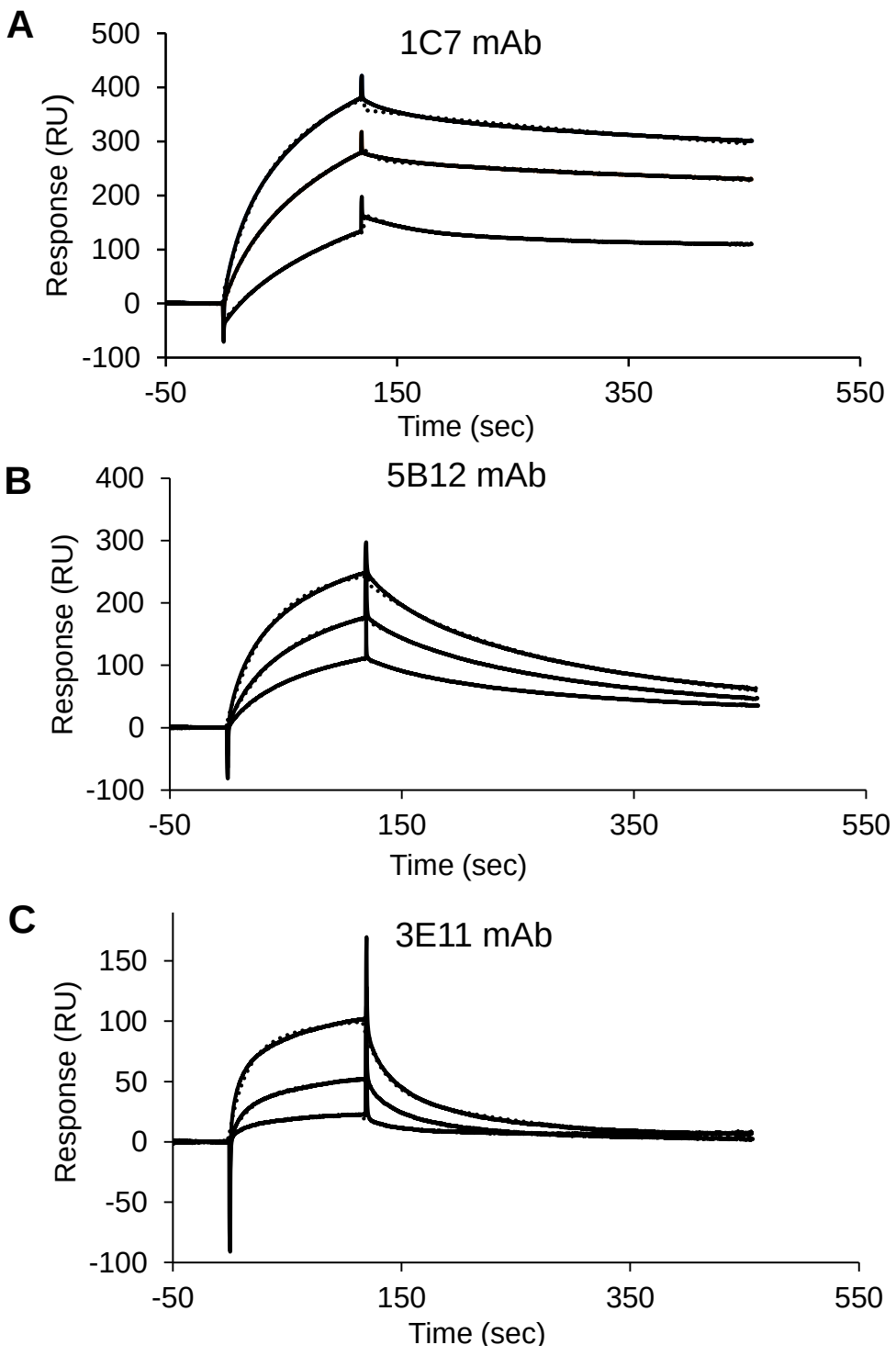

Figure 15: Binding properties of mAbs. (A) Kinetic analysis of 1C7 mAb (25 nM, 50 nM and 100 nM) binding to immobilized KIR2DS1. (B) Kinetic analysis of 5B12 mAb (52 nM, 105 nM and 210 nM) binding to immobilized KIR2DS1. (C) Kinetic analysis of 3E11 mAb (115 nM, 230 nM and 460 nM) binding to immobilized KIR2DS1.

Response curves (solid line) were fitted locally using a bivalent analyte model (dashed line).

Table 6. Calculated parameters of interaction between KIR2DS1 and mAbs (1C7, 5B12 and 3E11) by bivalent model in SPR analysis.

	k_{on} 1 (1/Ms)	k_{off} 1 (1/s)	k_{on} 2 (1/RUs)	k_{off} 2 (1/s)	R_{max} (RU)	Chi2
1C7 mAb						
0.1 μM	7.88×10^{4}	1.19×10^{-3}	0.0127	0.555	587	5.58
0.05 μM	9.28×10^{4}	0.0786	9.11×10^{-5}	3.34×10^{-4}	930	5.58
0.025 μM	7.4×10^{4}	0.0118	2.21×10^{-5}	3.9×10^{-4}	700	5.58
5B12 mAb						
0.21 μM	3.61×10^{4}	0.0104	7×10^{-4}	0.0537	433	3.47
0.105 μM	5.33×10^{4}	7.75×10^{-3}	2.66×10^{-5}	3.15×10^{-3}	326	3.47
0.0525 μM	8.04×10^{4}	8.83×10^{-3}	3.9×10^{-5}	2.27×10^{-3}	249	3.47
3E11 mAb						
0.460 μM	1.82×10^{4}	0.0492	3.06×10^{-5}	4.26×10^{-3}	324	3.78
0.230 μM	1.78×10^{4}	0.0397	2.55×10^{-5}	4.4×10^{-3}	257	0.391
0.115 μM	4.47×10^{4}	0.0272	7.84×10^{-5}	3.99×10^{-8}	65.3	0.159

2-3. The binding of Fabs to KIR2DS1 protein

To examine the monovalent binding characteristics of three mAbs with KIR2DS1 antigen, the Fabs of mAbs were used for SPR analysis. The Fabs were injected at a flow rate of 5 μL/min over the flow cells onto which biotinylated KIR2DS1 had been immobilized (around 1000 RU) at 25°C. Because the binding of the Fabs to KIR2DS1 showed fast dissociation in the preliminary experiment, the eq-binding analysis was performed. The sensorgrams of Fabs showed specific binding to immobilized KIR2DS1 concentration-dependently, and the binding responses were well fitted to the 1:1 langmuir binding model (Figure. 16).

The K_D values of Fab 1C7, 5B12, and 3E11 calculated by the 1:1 Langmuir binding model were 0.61 μM, 13 μM and 19 μM, respectively. Similar with the results of mAbs binding to the

KIR2DS1, the 1C7 Fab also has the highest affinity to the KIR2DS1. Thus, 1C7 clone was selected for the structural analysis and functional analysis.

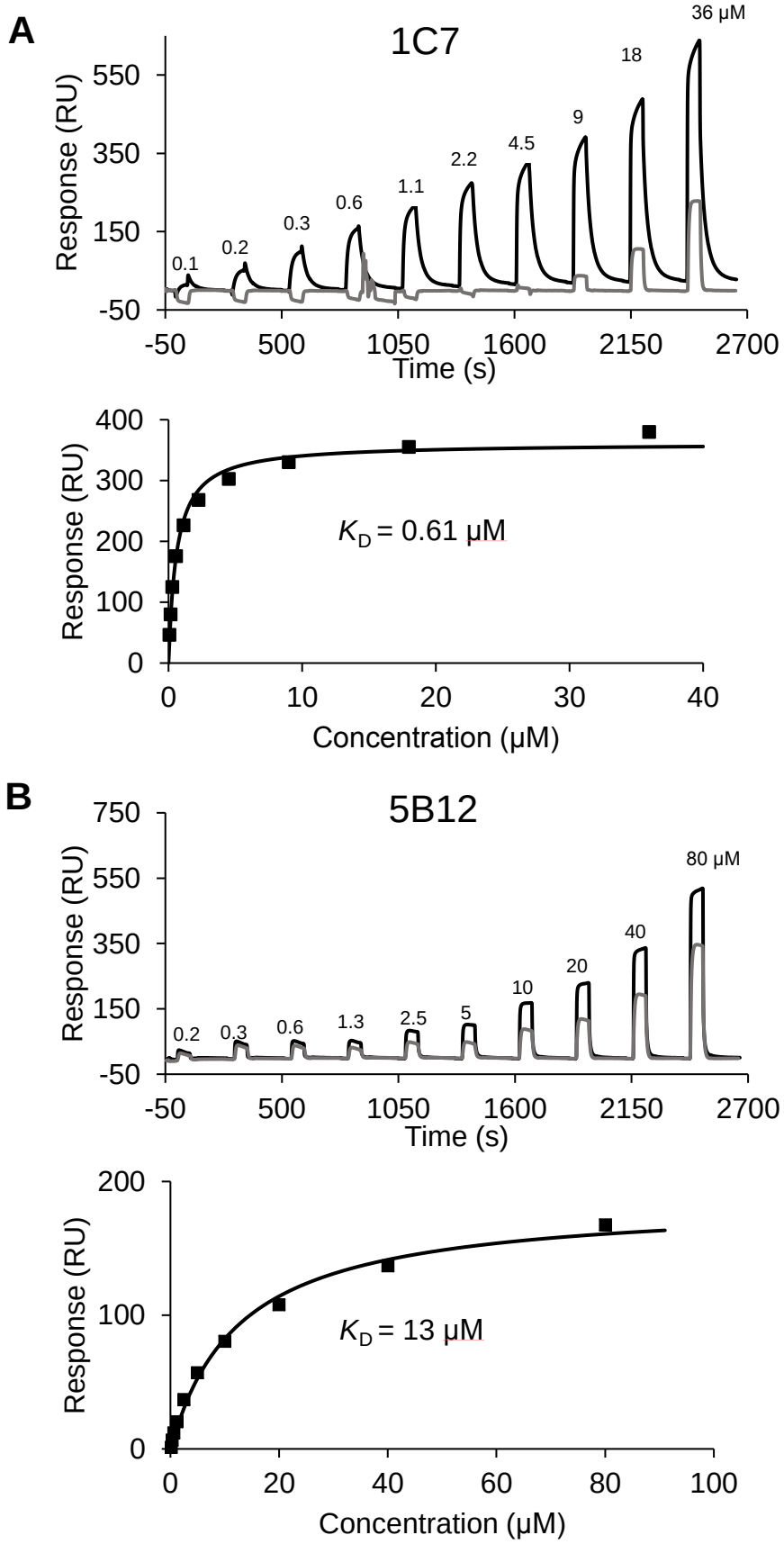

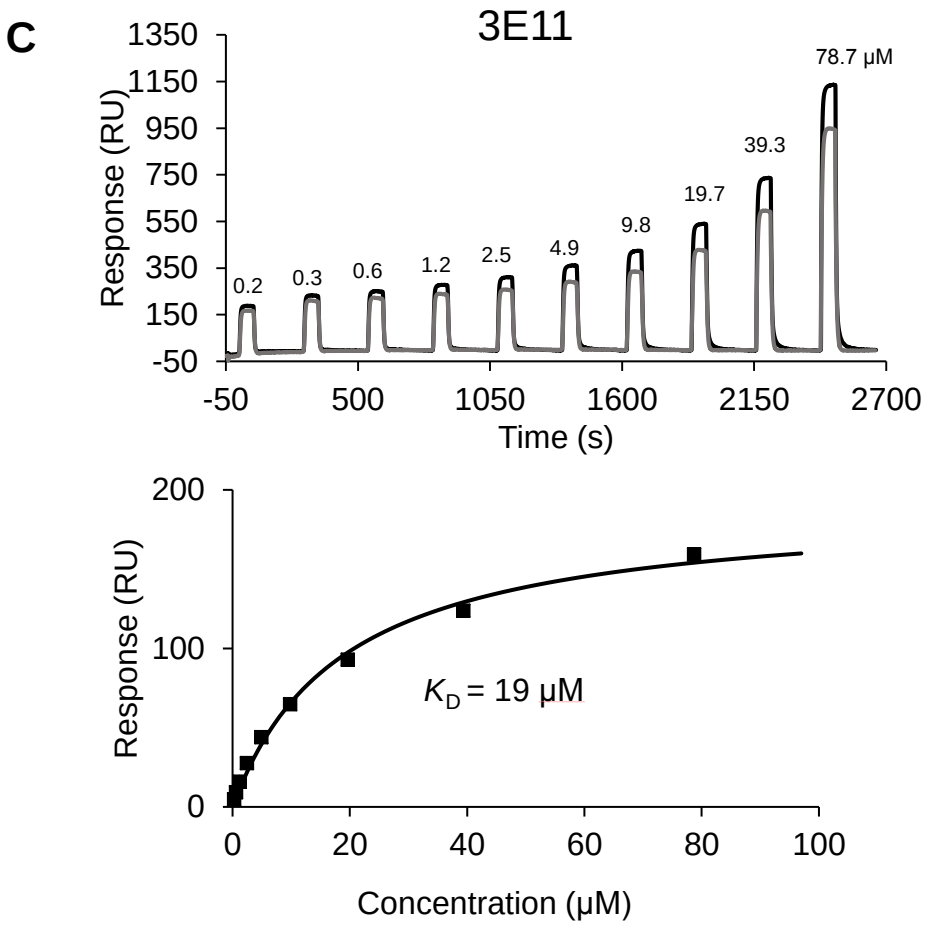

Figure 16: Equilibrium binding analysis of Fabs. The sensorgrams (upper) and the equilibrium binding fitting curves and K_D values (lower) of Fab fragments 1C7 (A), 5B12 (B) and 3E11 (C). The Fab fragments were injected at the indicated concentrations through flow cells with KIR2DS1 (black line) and control SA (gray line).

2-4. Thermodynamic analysis of three Fabs and KIR2DS1 interaction

To understand the thermodynamic properties of mAbs-KIR2DS1 binding, SPR analysis was performed. For this analysis, the serially diluted Fab fragments of three mAbs were injected over the immobilized KIR2DS1 (1000 mAU) at the different temperature (12°C, 15°C, 20°C, 25°C and 30°C), and the K_D values were determined under each temperature by equilibrium binding analysis. The results of 1C7 Fab-KIR2DS1 binding were shown in Figure 17 and the K_D values of three Fabs were summarized in Table 7.

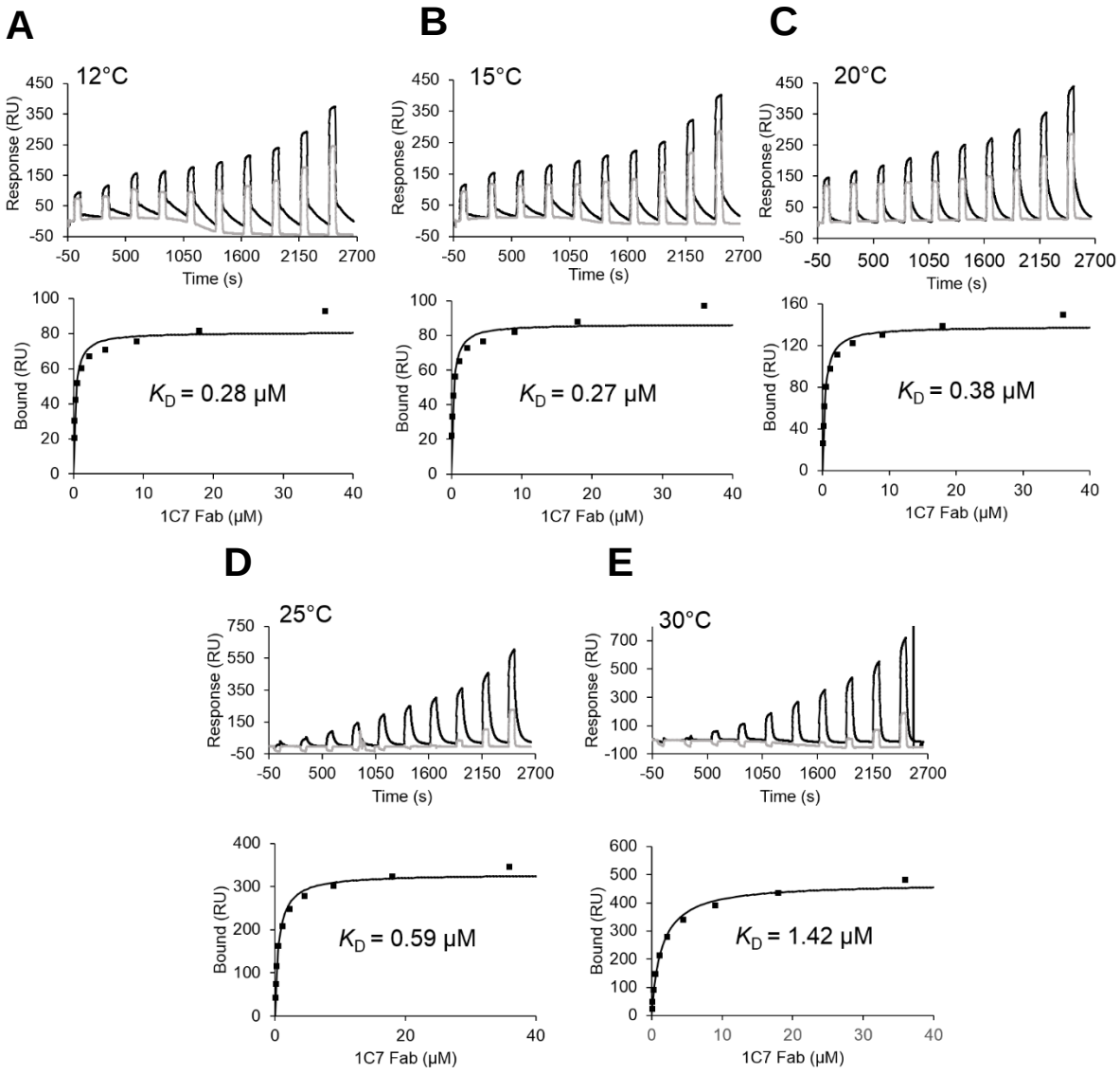

Figure 17. Equilibrium binding of 1C7 Fab at different temperatures. The sensorgrams (upper) and the equilibrium binding fitting curves and K_D values (lower) of 1C7 Fab-KIR2DS1 binding at 12°C (A), 15°C (B), 20°C (C), 25°C (D) and 30°C (E). The concentration of 1C7 Fab was as same as Figure 16A.

Table 7. The K_D values of three Fabs at the different temperatures.

Temperature	1C7	5B12	3E11
10°C	-	-	47.76 μM
12°C	0.28 μM	13.98 μM	41.32 μM
15°C	0.27 μM	14.76 μM	27.13 μM
20°C	0.38 μM	19.38 μM	23.84 μM
25°C	0.59 μM	29.61 μM	15.36 μM
30°C	1.42 μM	38.72 μM	17.23 μM

The thermodynamic parameters were obtained by van't Hoff analysis. The standard state Gibbs energy change (ΔG) were plotted against temperatures and fitted with non-linear van't Hoff equation (b). Binding enthalpy (ΔH), entropy (ΔS) and heat capacity (ΔC_p) were obtained simultaneously from these fitting results. The thermodynamic parameters of three Fabs-KIR2DS1 are summarized in Table 8 and Figure 18A. These parameters showed all three Fabs recognize KIR2DS1 spontaneously.

Table 8. Thermodynamic parameters of the interaction between three Fabs and KIR2DS1 at 25°C.

Immobilized	Analyte	n[a]	ΔG (kcal mol^{-1})	ΔH (kcal mol^{-1})	$-T\Delta S$ (kcal mol^{-1})	ΔC_p (kcal mol^{-1} K^{-1})
KIR2DS1	1C7[b]	3	-8.5 ± 0.03	-24 ± 0.8	15 ± 0.8	-1.9 ± 0.2
KIR2DS1	5B12[b]	3	-6.2 ± 0.05	-18 ± 2.1	12 ± 2.0	-1.1 ± 0.2
KIR2DS1	3E11[b]	3	-6.6 ± 0.04	2.4 ± 2.7	-8.9 ± 2.7	-1.1 ± 0.1

For the data from SPR analysis, ΔG, ΔH, $-T\Delta S$, ΔC_p represent binding changes in standard state Gibbs energy, enthalpy, entropy and heat capacity, respectively, calculated with non-linear van't Hoff equation.

[a]n, numbers of experiments.

[b]The values are means ± standard deviation derived from multiple experiments.

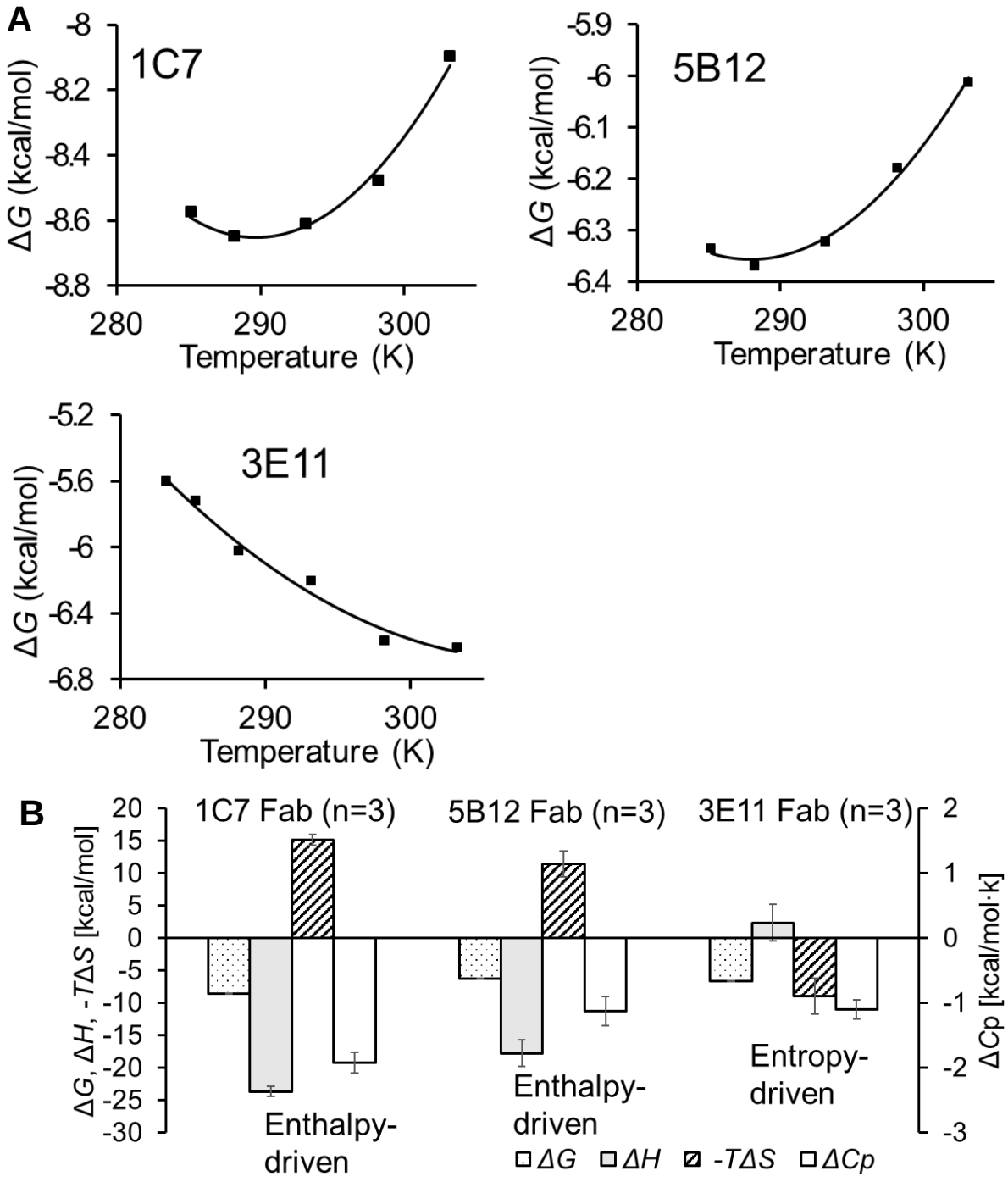

Figure 18. Thermodynamics of three Fabs-KIR2DS1. (A) The representative plots of three Fabs-KIR2DS1 temperature dependency of binding Gibbs energy (Δ*G*) determined by SPR experiments. Gibbs energies at five temperature points (12°C, 15°C, 20°C, 25°C and 30°C) were obtained from K_D values from equilibrium binding analysis. (B) Comparison of thermodynamic properties (at 25℃) of three Fabs-KIR2DS1 interactions. Error bars represent standard error of the mean.

The recognition of KIR2DS1 by 1C7 Fab and 5B12 Fab showed similar thermodynamic characteristics, the enthalpy-driven force with the unfavorable entropy and a large heat capacity change (Figure 18B). These binding characters suggested the induced-fit binding with conformational adjustments and with a reduction in flexibility. On the other hand, 3E11 Fab-KIR2DS1 binding showed the entropy-driven binding with a small enthalpy gain and a heat capacity change (Figure 18B). Favorable entropic changes suggested a rigid-body interaction and limited conformational changes accompany the binding. The binding enthalpy of 1C7 Fab/5B12 Fab-KIR2DS1 was similar to the other antigen-antibody interactions, which suggests a large net increase in the number of favorable noncovalent bonds (e.g., hydrogen bonds and Van der Waals contacts) following binding.

3. The structural analysis of 1C7 Fab

From the SPR analyses, 1C7 mAb showed the highest affinity to KIR2DS1 with slow dissociation and its interaction was suggested to be the enthalpy driven. Thus, 1C7 mAb was expected to be a possible candidate for clinical application. To understand the molecular recognition mechanism at the atomic level and to perform further optimization of CDR sequences of 1C7, the X-ray crystallization analysis of 1C7 Fab and 1C7/KIR2DS1 complex were performed. Unfortunately, crystallographic data of the complex of 1C7Fab with KIR2DS1 has not been obtained so far. However, the crystals of 1C7 Fab were obtained in the reservoir buffer; 0.1M Tris pH 8.5, 30% (w/v) PEG1000 (Figure 19A). The X-ray diffraction data set was collected on the beamline BL17A of the Photon Factory (Tsukuba, Japan). The 1C7 Fab structure was solved by the molecular replacement method at 2.00 Å resolution using the VH and VL regions of a Fab (PDB codes: 1NCW and 4M1G) as search models for VH and VL, respectively. The model of 1C7 Fab was refined until the value of R_{work} and R_{free} factors converged using refinement programs. The data collection and processing statistics are summarized in Table 9.

The overall structure of 1C7Fab showed a typical Fab fragment fold (Figure 19B), with some flexible loops which was not visible in the electron density map and thus disordered. This is consistent with the typical antigen-antibody binding property, the flexible region of CDRs contribute to the binding of the antigen.

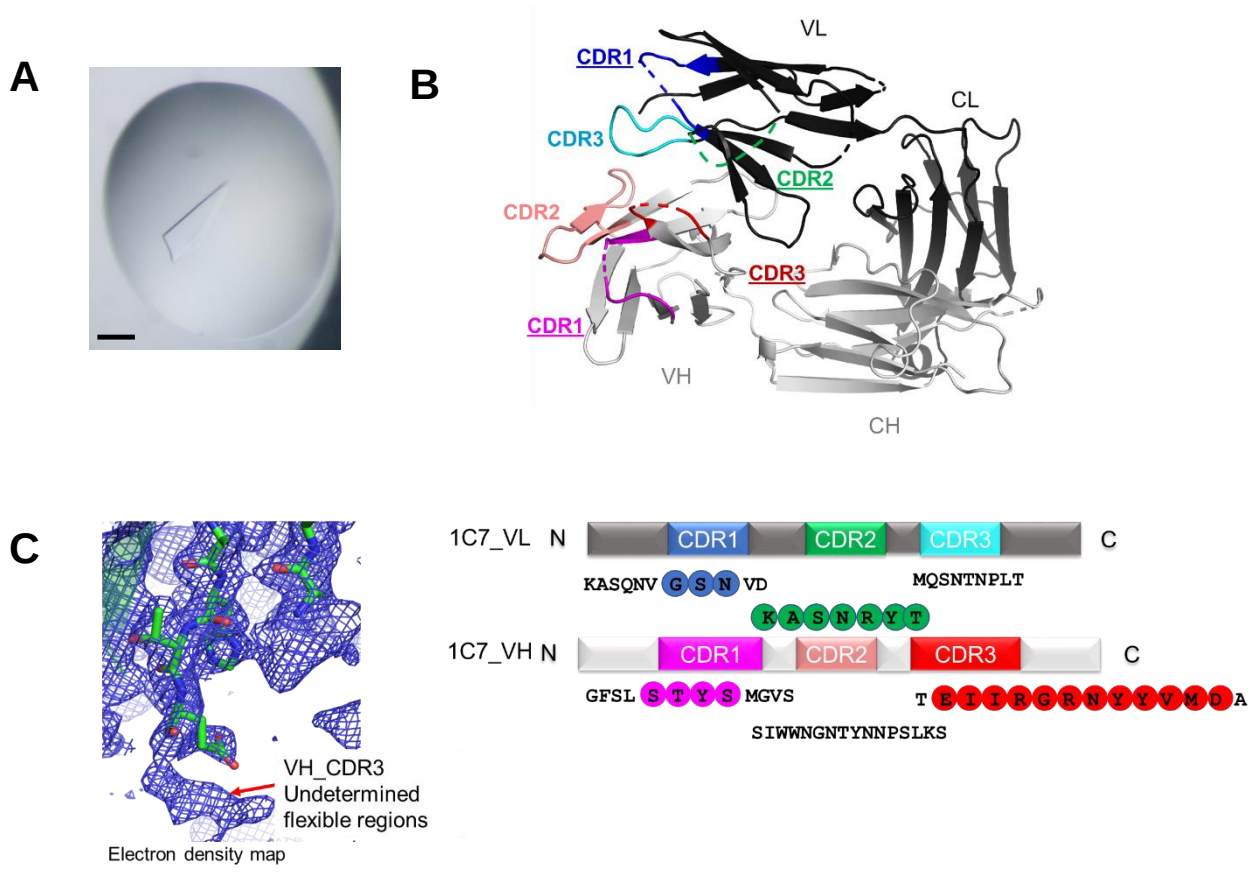

Figure 19: Crystallization of 1C7 Fab. (A) The picture of the 1C7 Fab protein crystals. The black bar indicates 100 μm. (B) The ribbon diagram of 1C7 Fab. The H and L chains are colored in light gray and dark gray, respectively. The invisible CDR region was shown by the dashed line. The VH CDR1, 2, 3 are colored in magenta, wheat and red, respectively. The VL CDR 1, 2, 3 are colored in blue, green and cyan, respectively. (C) The left is the electron density map of part of VH_CDR3. The red arrow pointed the electron density map regions of the undetermined flexible regions. The right is CDR sequences of 1C7 Fab. The amino acids in the colored circles are the structurally undetermined flexible regions.

Table 9. Data collection and refinement statistics

Data collection	**1C7 Fab**
wavelength (Å)	1.00
resolution (Å)	2.00
space group	C1 2 1
unit-cell parameters (Å)	a=161.042
	b=41.863
	c=60.355
multiplicity	3.4 (3.5)
completeness (%)	99.52 (98.79)
$\langle I/\sigma(I)\rangle$	11.85 (1.88)
R_{sym}	0.07132 (0.6958)
unique reflections	27386 (2686)
Refinement	
resolution (Å)	46.5-2.0
R_{work}/R_{free}	0.2761/0.3180
Number of atoms	3054
macromolecules	2954
water	100
RMSD	
Bond length (Å)	0.0033
Bond angle (°)	0.68
Ramachandran (%)	
favored	94.07
allowed	4.85
outliers	1.08
Mean B-factor (Å^2)	50.23
macromolecules	50.45
solvent	43.65

Discussion

In this study, the crystal structure of KIR2DS1 has been determined at 3.92 Å (Figure 10), and the D1 and D2 domains form a V-shaped orientation, as revealed from the crystal structures of other KIR2Ds [22, 34, 35]. This means KIR2DS1 binds the cognate ligand, group 2 HLA-C, using the same hinge region as shown in the KIR2DL1/HLA-Cw4, KIR2DL2/HLA-Cw3 and KIR2DS2/HLA-A11 complex (Figure 4B). This highly conserved structure of KIR2Ds would be essential to recognize both HLA-C heavy chain and the C-terminal region of a peptide. Regarding the especially for the difference of N80 and K80 which determine the group of HLA-C, the superimpose of KIR2DL1/HLA-Cw4 to KIR2DL2/HLA-Cw3 structure showed that many of the residues conserved in these KIR2DLs and HLA-Cs mediate different interactions in the KIR2DL1–HLA-Cw4 and KIR2DL2–HLA-Cw3 complexes [34]. The resolution of the KIR2DS1 crystal structure in the present study was not enough to discuss on the orientation of the side chain. Therefore, higher resolution structure of KIR2DS1 and/or complex structures of KIR2DS1/HLA-C will be necessary to reveal how the limited differences of amino acid sequences between activating KIR2DS1 and KIR2DS2 cause the ligand specificity. On the other hand, the paired inhibitory receptors generally showed higher affinity to their self-ligands than the paired activating receptors to suppress the unnecessary immune response against the normal cells. For example, the K_D value of KIR2DL1/HLA-Cw4 is 7.2 μM, of KIR2DS1/HLA-Cw4 is 30 μM [21]. The complex structure of KIR2DS1/HLA-Cw4 will be able to explain the difference of their binding affinity to HLA-C ligands in future.

In regards of the recognition of KIR2DS1 by three novel specific antibodies, the region around the possible epitopes, N163 and T154, also had no apparent structural changes compared with the KIR2DL1structure (Figure 10). It is suggested that the specific recognition of three anti-KIR2DS1 antibodies might not be related to the structural change between KIR2DS1 and KIR2DL1 but be directly dependent on N163 and T154 residues. It is consistent with the previous result of western blotting analysis of five KIR2D proteins which showed the specificity of all three mAbs to KIR2DS1. Thus, our novel three specific mAbs for KIR2DS1 could be used for detection of both denatured and folded KIR2DS1 in the basic research experiment. Importantly, all reported KIR2DS1 polymorphic alleles possess these two amino acid residues contributed to the specificity of mAbs. Therefore, these mAbs could be also used for the detection of serum or cell surface expression levels of all KIR2DS1 allele products and applied for clinical use as therapeutic reagents targeting KIR2DS1 in human individuals.

1C7 mAb showed the highest affinity to KIR2DS1 in SPR analyses (Figure 15) and was suggested to use wider epitopes including both N163 and T154 than the others (N163 only) in the previous study. In the CDR region, 1C7 has unique amino acid sequences especially in CDR3 of heavy chain (Table 3). From the observation of comprehensive protein-protein interactions of dimeric proteins, some preference of amino acids for protein-protein interaction at the interfaces were summarized [52]. For example, some polar residues, asparagine (N) and arginine (R), have a particular affinity for the interface, and nonpolar methionine (M) and proline (P) were slightly preferred in interfaces. Tyrosine (Y) was favored in interfaces, while phenylalanine (F) and tryptophan (W) were not [52]. 1C7 VH_CDR3 has more favored residues, asparagine (N) and arginine (R), than the other two clones, 5B12 and 3E11 (Table 3). They might play important roles for KIR2DS1 binding with higher affinity. Since the 1C7 Fab-KIR2DS1 is enthalpy-driven binding with the unfavorable binding entropy (Figure 18B), it might create a large net increase in the number of favorable noncovalent bonds (e.g., hydrogen bonds, van der Waals contacts and salt bridge) following the antigen binding [53]. Most antibody/protein interactions reported so far have much more unfavorable binding entropies and more favorable binding enthalpies than other general protein-protein interactions such as receptor-ligand interactions [54]. Therefore, the clone 1C7-KIR2DS1 binding is one of the typical antigen-antibody interactions with the highest affinity and enthalpically-driven force.

In the comparison between 3E11 and 5B12 mAbs, only five different amino acid residues in the VH_CDR3 were observed. However, these two mAbs showed opposite thermodynamics for KIR2DS1 binding; 5B12 showed the enthalpy-driven recognition but 3E11 showed the entropy-driven binding with the fastest dissociation rate (Figure 15, 18). In the VH_CDR3 of 3E11, the proline (P) of might have less flexibility and the phenylalanine (F) is not favored on the interface due to its hydrophobic side chain. On the opposite, the histidine (H) in the VH_CDR3 of 5B12 is one of the most favored on the interface [54]. A slight concave surface might be built on the VH_CDR3 loop of 3E11, however, 5B12 might have softer and more flexible loop (Figure 20). The entropy driven binding of 3E11 to KIR2DS1 also suggested a rigid-body interaction and limited conformational changes accompany the binding. The high similarity of CDR sequences of three mAbs would be essential for KIR2DS1-specific binding because other non-specific anti-KIR2DS1 mAbs (bind to all KIR2Ds) showed quite variable length and sequences in all CDRs (data not shown). However, the few different residues of VH_CDR3 could affect the binding property of mAbs. Therefore, 3E11 clone might not be suitable to be improved for clinical application.

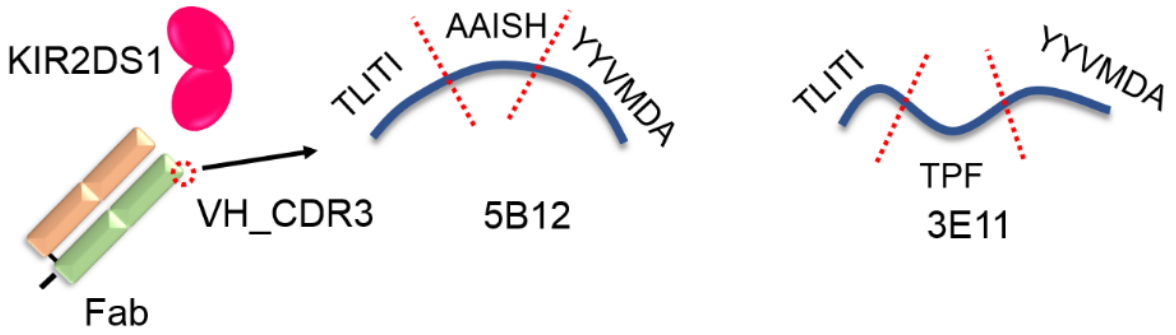

Figure 20: The schematic diagram of 5B12 and 3E11 VH_CDR3s.

From the results of SPR analyses, I considered that 1C7 mAb might be preferable for future clinical application. The crystal structure of 1C7 Fab fragment clearly showed the existence of the flexible region of CDRs. Such a flexibility of CDRs always play an important role on the specific binding. In the crystal structure of 1C7 fab, the VL_CDR2 and VH_CDR3 showed flexible regions (Figure 19) and can contribute to the "induced-fit" binding with conformational changes [55, 56]. The thermodynamic and affinity analyses revealed that the VH_CDR3 already be pointed a meaningful role for the specificity binding. The CDR3 region of heavy chains was reported to be important for the specific recognition but not sufficient for the whole specific binding and it needs to cooperate with other CDRs of light chains [57]. I considered that the VH_CDR3 conformational change of 1C7 is accompanied by conformational changes in the VL_CDR2, which have a less intimate involvement in the Fab-KIR2DS1 interface.

As described above, 1C7 might recognize KIR2DS1 using the different surface area of KIR2DS1. The flexible loops in the VH_CDR3 and VL_CDR2 regions of 1C7 Fab, which contain the flexible region for the specific binding with a conformational change (Figure 21), would be directly used for the N163 and T154 recognition, respectively (Figure 21). In the 1C7-KIR2DS1 binding, the same CDR2 of the light chains among three mAbs might have a role on binding to KIR2DS1 N163 and the variable CDR3 of the heavy chain might have an important role on the binding to KIR2DS1 T154.

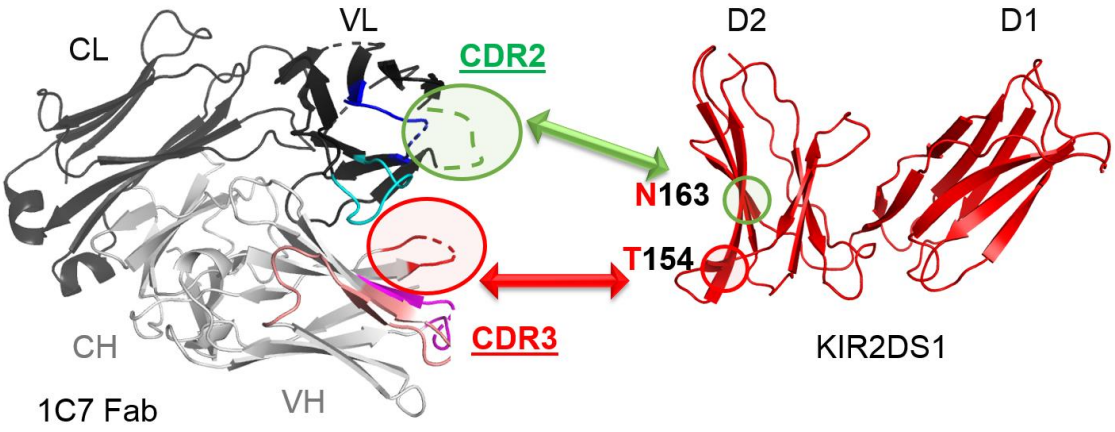

The non-specific KIR2DS1 antibodies (e.g., Lirilumab) might target the common region of KIR2Ds, therefore they could not recognize the different ligand specifically. That might be the reason why Lirilumab failed at phase 2. Our mAbs can specifically recognize the KIR2DS1 molecules, they might get over that problem and become promising KIR2DS1-targed drug candidates. I am also interested in whether the binding of three monoclonal antibodies would be competitive with HLA class I molecules to KIR2DS1 or not. The possible binding epitopes, including N163 and T154, are located in the domain 2 of KIR2DS1 and seemed to be different region from the HLA class I binding area, the KIR2D hinge region between D1 and D2. In the preliminary competitive binding SPR analysis, all three mAbs partially inhibited the binding of HLA-C to KIR2DS1 probably due to the steric hindrance by mAbs. Further investigation will be required to clarify the inhibition mechanism of the mAbs, especially 1C7 mAb, and the function of three antibodies at the cellular level and in vivo. Moreover, further optimal modification of 1C7 CDRs to acquire the higher affinity to KIR2DS1 keeping its specificity by introducing mutations that stabilize the binding configuration with reducing the entropic penalty of binding and increasing the affinity [53, 58] will be expected for the basic and the clinical application.

The genes encoding inhibitory *KIR*s are nearly always present in populations at frequencies greater than 90% to avoid the immune activation against self-healthy cells expressing HLA class I. However, activating *KIR* show much greater variation in their presence/absence in different populations. For example, *KIR2DS1* has four populations with greater than 80% frequency (Australia Aborigines, Brazil Amazon, Brazil Rodonia Province

Karitiana and Papua New Guinea Nasioi) but three African populations with < 10%; Central Africa Republic Bagandu Biaka, Ghana and Nigeria Enugu Ibo [59]. In Japan, 14 of 50 (28%) healthy controls and 43 of 96 (45%) psoriasis vulgaris (PV) patients are *KIR2DS1*-positive [60]. Interestingly, *KIR2DS1* also showed the most significant increase in psoriatic arthritis among KIR families [61]. KIR2DS1 has been genetically reported to be associated with many other diseases, for example, endometriosis, Vogt-Koyanagi-Harada disease, diabetes mellitus type 1 and lupus erythematosus systemic by genetic analyses. However, the expression level of KIR2DS1 has not been clearly determined because any anti-KIR2DS1 specific antibody has not been available. Our novel anti-KIR2DS1 specific antibodies are expected to be used to survey the KIR2DS1 expression level in the disease patients and the relationship with the disease progression. The novel therapy that modifies the immune functions through KIR2DS1 might be important for broad diseases. Therefore, the optimized anti-KIR2DS1 specific antibodies will be expected to be applied to KIR2DS1-positive patients of broad immune-disordered diseases as clinical applications and /or reagents for companion diagnostics.

References

1. Vivier, E., Tomasello, E., Baratin, M., Walzer, T. & Ugolini, S. Functions of natural killer cells. Nat. Immunol. 9, 503–510 (2008).

2. Bashirova, A. A., Martin, M. P., McVicar, D. W. & Carrington, M. The Killer Immunoglobulin-Like Receptor Gene Cluster: Tuning the Genome for Defense. Annu. Rev. Genomics Hum. Genet. 7, 277–300 (2006).

3. Ljunggren HG, Karre K. In search of the "missing self": MHC molecules and NK cell recognition. Immunol. *Today* 11:237–44 (1990).

4. Kuroki, K., Furukawa, A. & Maenaka, K. Molecular recognition of paired receptors in the immune system. Front. Microbiol. 3, 1–12 (2012).

5. Barrow, A. D., Martin, C. J. & Colonna, M. The natural cytotoxicity receptors in health and disease. Front. Immunol. 10, 1–20 (2019).

6. Pende, D. et al. Killer Ig-like receptors (KIRs): Their role in NK cell modulation and developments leading to their clinical exploitation. Front. Immunol. 10, (2019).

7. Anegón, I., Cuturi, M. C., Trinchieri, G. & Perussia, B. Interaction of Fc receptor (CD16) ligands induces transcription of interleukin 2 receptor (CD25) and lymphokine genes and expression of their products in human natural killer cells. J. Exp. Med. 167, 452–472 (1988).

8. Bar-On, Y., Seidel, E., Tsukerman, P., Mandelboim, M. & Mandelboim, O. Influenza virus uses its neuraminidase protein to evade the recognition of two activating NK cell receptors. J. Infect. Dis. 210, 410–418 (2014).

9. Colonna, M. et al. Alloantigen recognition by two human natural killer cell clones is associated with HLA-C or a closely linked gene. Proc. Natl. Acad. Sci. U. S. A. 89, 7983–7985 (1992).

10. Bauer, S. et al. Activation of NK cells and T cells by NKG2D, a receptor for stress-inducible MICA. Science 285, 727–729 (1999).

11. Cosman, D. et al. ULBPs, novel MHC class I-related molecules, bind to CMV glycoprotein UL16 and stimulate NK cytotoxicity through the NKG2D receptor. Immunity 14, 123–133 (2001).

12. Lanier, L. L., Corliss, B., Wu, J. & Phillips, J. H. Association of DAP12 with activating CD94/NKG2C NK cell receptors. Immunity 8, 693–701 (1998).

13. Braud, V. et al. HLA-E binds to natural killer cell receptors CD94/NKG2A, B and C. Nature 391, 795–799 (1998).

14. Lee, N. et al. HLA-E is a major ligand for the natural killer inhibitory receptor CD94/NKG2A. Proc. Natl. Acad. Sci. U. S. A. 95, 5199–5204 (1998).

15. Cosman, D. et al. A novel immunoglobulin superfamily receptor for cellular and viral MHC class I molecules. Immunity 7, 273–282 (1997).

16. Vivier, E., Nunès, J. A. & Vély, F. Natural killer cell signaling pathways. Science. 306, 1517–1519 (2004).

17. Moretta, A., Sun, P. D., Ugolini, S. & Vivier, E. Recognition of peptide – MHC class I complexes by activating killer immunoglobulin-like receptors. 102, (2005).

18. Wilson, M. J. et al. Plasticity in the organization and sequences of human KIR/ILT gene families. Proc. Natl. Acad. Sci. U. S. A. 97, 4778–4783 (2000).

19. Cisneros, E. et al. Haplotype-Based Analysis of KIR-Gene Profiles in a South European Population—Distribution of Standard and Variant Haplotypes, and Identification of Novel Recombinant Structures. Front. Immunol. 11, 1–15 (2020).

20. Hsu KC, Liu XR, Selvakumar A, Mickelson E, O'Reilly RJ, Dupont B. Killer Ig-like receptor haplotype analysis by gene content: evidence for genomic diversity with a minimum of six basic framework haplotypes, each with multiple subsets. J Immunol. (2002) 169:5118–29. doi: 10.4049/jimmunol.169.9.5118.

21. Maenaka, K., Juji, T., Stuart, D. I. & Jones, E. Y. Crystal structure of the human p58 killer cell inhibitory receptor (KIR2DL3) specific for HLA-Cw3-related MHC class I. Structure 7, 391–398 (1999).

22. Boyington, J. C., Motyka, S. a, Schuck, P., Brooks, a G. & Sun, P. D. Crystal structure of an NK cell immunoglobulin-like receptor in complex with its class I MHC ligand. Nature 405, 537–543 (2000).

23. Hilton HG, Guethlein LA, Goyos A, Nemat-Gorgani N, Bushnell DA, Norman PJ, et al. Polymorphic HLA-C receptors balance the functional characteristics of KIR haplotypes. J Immunol. 195:3160–70. doi: 10.4049/jimmunol.1501358 (2015).

24. Moesta AK, Norman PJ, Yawata M, Yawata N, Gleimer M, Parham P. Synergistic polymorphism at two positions distal to the ligand-binding site makes KIR2DL2 a stronger receptor for HLA-C than KIR2DL3. J Immunol. 180:3969–79. doi: 10.4049/jimmunol.180.6.3969 (2008).

25. Liu, J., Xiao, Z., Ko, H. L., Shen, M. & Ren, E. C. Activating killer cell immunoglobulin-like receptor 2DS2 binds to HLA-A*11. Proc. Natl. Acad. Sci. 111, 2662–2667 (2014).

26. Moretta, A., Sun, P. D., Ugolini, S. & Vivier, E. Recognition of peptide – MHC class I complexes by activating killer immunoglobulin-like receptors. 102, (2005).

27. VandenBussche CJ, Mulrooney TJ, FrazierWR, Dakshanamurthy S, Hurley CK. Dramatically reduced surface expression of NK cell receptor KIR2DS3 is attributed to multiple residues throughout the molecule. Genes Immun. 10:162–73. doi: 10.1038/gene.2008.91 (2009).

28. Bottino C, Sivori S, Vitale M, Cantoni C, Falco M, Pende D, et al. A novel surface molecule homologous to the p58/p50 family of receptors is selectively expressed on a subset of human natural killer cells and induces both triggering of cell functions and proliferation. Eur J Immunol. 26:1816–24. doi: 10.1002/eji.1830260823 (1996).

29. Chiesa, M. Della et al. Evidence that the KIR2DS5 gene codes for a surface receptor triggering natural killer cell function. 2284–2289 doi:10.1002/eji.200838434 (2008).

30. Graef, T. et al. KIR2DS4 is a product of gene conversion with KIR3DL2 that introduced specificity for HLA-A * 11 while diminishing avidity for HLA-C. J. Exp. Med. 206, 2557–2572 (2009).

31. Garcia-Beltran WF, Holzemer A, Martrus G, Chung AW, Pacheco Y, Simoneau CR, et al. Open conformers of HLA-F are high-affinity ligands of the activating NK-cell receptor KIR3DS1. Nat Immunol. 17:1067–74. doi: 10.1038/ni.3513 (2016).

32. Burian A, Wang KL, Finton KA, Lee N, Ishitani A, Strong RK, et al. HLA-F and MHC-I open conformers bind natural killer cell Ig-like receptor KIR3DS1. PLoS ONE. 11: e0163297. doi: 10.1371/journal.pone.0163297 (2016).

33. Carlomagno S, Falco M, Bono M, Alicata C, Garbarino L, Mazzocco M, et al. KIR3DS1-mediated recognition of HLA-∗B51: modulation of KIR3DS1 responsiveness by selfHLA-B allotypes and effect onNKcell licensing. Front. Immunol. 8:581. doi: 10.3389/fimmu.2017.0058 (2017).

34. Fan, Q. R., Long, E. O. & Wiley, D. C. Crystal structure of the human natural killer cell inhibitory receptor KIR2DL1-HLA-Cw4 complex. Nat. Immunol. 2, 452–460 (2001).

35. Saulquin, X., Gastinel, L. N. & Vivier, E. Crystal Structure of the Human Natural Killer Cell Activating Receptor KIR2DS2 (CD158j). J. Exp. Med. 197, 933–938 (2003).

36. Smita Kulkarnia. et al. The Ying and Yang of HLA and KIR in Human Disease. Bone 23, 1–7 (2008).

37. Alter G, Martin MP, Teigen N, Carr WH, Suscovich TJ, Schneidewind A, et al. Differential natural killer cell-mediated inhibition of HIV-1 replication based on distinct KIR/HLA subtypes. J Exp Med. 204(12):3027–36 (2007).

38. Winter CC, Gumperz JE, Parham P, Long EO, Wagtmann N. Direct binding and functional transfer of NK cell inhibitory receptors reveal novel patterns of HLA-C allotype recognition. J Immunol. 161(2):571–7 (1998).

39. Ahlenstiel G, Martin MP, Gao X, Carrington M, Rehermann B. Distinct KIR/HLA compound genotypes affect the kinetics of human antiviral natural killer cell responses. J Clin Invest. 118(3):1017–26 (2008).

40. Cook M, Briggs D, Craddock C, Mahendra P, Milligan D, Fegan C, et al. Donor KIR genotype has a major influence on the rate of cytomegalovirus reactivation following T-cell replete stem cell transplantation. Blood. 107(3):1230–2 (2006).

41. Namekawa T, Snyder MR, Yen JH, Goehring BE, Leibson PJ, Weyand CM, et al. Killer cell activating receptors function as costimulatory molecules on CD4+CD28null T cells clonally expanded in rheumatoid arthritis. J Immunol. 165(2):1138–45 (2000).

42. Naumova E, Mihaylova A, Stoitchkov K, Ivanova M, Quin L, Toneva M. Genetic polymorphism of NK receptors and their ligands in melanoma patients: prevalence of inhibitory over activating signals. Cancer Immunol Immunother. 54(2):172–8 (2005).

43. Naumova E, Mihaylova A, Ivanova M, Mihailova S. Impact of KIR/HLA ligand combinations on immune responses in malignant melanoma. Cancer Immunol Immunother. 56(1):95–100 (2007).

44. Verheyden S, Bernier M, Demanet C. Identification of natural killer cell receptor phenotypes associated with leukemia. Leukemia. 18(12):2002–7 (2004).

45. Besson C, Roetynck S, Williams F, Orsi L, Amiel C, Lependeven C, et al. Association of killer cell immunoglobulin-like receptor genes with Hodgkin's lymphoma in a familial study. PLoS ONE. 2(5):e406 (2007).

46. Pende, D. et al. Killer Ig-like receptors (KIRs): Their role in NK cell modulation and developments leading to their clinical exploitation. Front. Immunol. 10, (2019).

47. Vey, N. et al. A phase I trial of the anti-inhibitory KIR monoclonal antibody IPH2101 for acute myeloid leukemia (AML) in complete remission. Blood 120, 1–3 (2012).

48. Van Der Weyden C, Bagot M, Neeson P, Darcy PK, Prince HM. IPH4102, a monoclonal antibody directed against the immune receptor molecule KIR3DL2, for the treatment of cutaneous T-cell lymphoma. Expert Opin Investig Drugs. 27:691–7. doi: 10.1080/13543784.2018. 1498081(2018).

49. Bahler DW, Hartung L, Hill S, Bowen GM, Vonderheid EC. CD158k/KIR3DL2 is a useful marker for identifying neoplastic T-cells in Sezary syndrome by flow cytometry. Cytometry B Clin Cytom. 74B (3):156–62 (2007).

50. Bagot, M. et al. IPH4102, a first-in-class anti-KIR3DL2 monoclonal antibody, in patients with relapsed or refractory cutaneous T-cell lymphoma: an international, first-in-human, open-label, phase 1 trial. Lancet Oncol. 20, 1160–1170 (2019).

51. Shiroishi, M. et al. Human inhibitory receptors Ig-like transcript 2 (ILT2) and ILT4 compete with CD8 for MHC class I binding and bind preferentially to HLA-G. Proc. Natl. Acad. Sci. U. S. A. 100, 8856–8861 (2003).

52. Jones S, Thornton Jm. Protein-protein interactions: a review of protein dimer structures. Prog Biophys Mol Biol 63(1):31-65 (1995).

53. Willcox, B. E. et al. TCR binding to peptide-MHC stabilizes a flexible recognition interface. Immunity 10, 357–365 (1999).

54. Stites, W. E. Protein-protein interactions: Interface structure, binding thermodynamics, and mutational analysis. Chem. Rev. 97, 1233–1250 (1997).

55. Oda, M., Furukawa, K., Ogata, K., Sarai, A., and Nakamura, H. Thermodynamics of specific and non-specific DNA binding by the c-Myb DNA-binding domain. J. Mol. Biol. 276, 571-590 (1998).

56. Masayuki Oda. Equilibrium Association Constant: **4**, 45–56 (2004).

57. D'Angelo, S. et al. Many routes to an antibody heavy-chain CDR3: Necessary, yet insufficient, for specific binding. Front. Immunol. 9, 1–13 (2018).

58. Wedemayer, G.J., Patten, P.A., Wang, L.H., Schultz, P.G., and Ste- vens, R.C. Structural insights into the evolution of an anti- body combining site. Science 276, 1665–1669 (1997).

59. Middleton, D. & Gonzelez, F. The extensive polymorphism of KIR genes. Immunology 129, 8–19 (2010).

60. Suzuki, Y. et al. Genetic polymorphisms of killer cell immunoglobulin-like receptors are associated with susceptibility to psoriasis vulgaris. J. Invest. Dermatol. 122, 1133–1136 (2004).

61. Nelson GW, Martin MP, Gladman D, Wade J, Trowsdale J, Carrington M. Cutting edge: heterozygote advantage in autoimmune disease: hierarchy of protection/susceptibility conferred by HLA and killer Ig-like receptor combinations in psoriatic arthritis. J Immunol. 173(7):4273– 6 (2004).

Acknowledgements

I would first like to thank my supervisors, Professor Katsumi Maenaka and Associate Professor Kimiko Kuroki. Thank you so much for giving me the important opportunity to start this new project and giving me the advices to complete it. I would never forget your kindness in the whole life.

I would like to thank for Dr Shunsuke Kita and Dr Haruki Matsubara. Thank you for teaching me how to do the experiments of protein crystallization and analyze the data of protein crystal. I really learned a lot of useful technics from you.

I would like to acknowledge all the staff and members of the Biomolecular Science laboratory and Center for Research and Education on Drug Discovery, Faculty of Pharmaceutical Sciences, Hokkaido University. Thank you always willing to help me. Thank you for comparing me and supporting me just like my families, let me have a wonderful life in Hokkaido, Japan.

I would like to thank Professor Akio Kihara and Appointed Associate Professor Naoyoshi Maeda. Thank you for giving me the comments about this paper.

I would like to thank my parents for their wise counsel and sympathetic ear. You are always there for me. Finally, there are my friends, who were of great support in deliberating over our problems and findings.